hydrology

MDPI

Review

Advancing the Use of Satellite and Reanalysis Precipitation Data in Data-Scarce High-Altitude Regions: A Comprehensive Review

Liangkun Deng [1,2,3], Shihan Shan [1,*], Hua Chen [2], Xiang Zhang [2], Guiliang Zhong [1], Fuling Wen [1] and Yan Zhang [1]

1 PowerChina Chengdu Engineering Corporation Limited, Chengdu 610072, China
2 State Key Laboratory of Water Resources Engineering and Management, Wuhan University, Wuhan 430072, China
3 School of Computer Science, China University of Geosciences, Wuhan 430078, China
* Correspondence: sshihan@chidi.com.cn

Highlights

What are the main findings?

- This study presents a thorough and holistic review of the advances, limitations, and future directions in utilizing satellite and reanalysis precipitation products to overcome data scarcity, with particular emphasis on high-altitude regions.
- These precipitation products exhibit non-negligible systematic biases and pronounced conditional biases across spatial, seasonal, and daily scales in high-altitude regions, requiring bias correction and data merging to improve accuracy.

What are the implications of the main findings?

- Further advancements in the application of precipitation products over high-altitude regions require addressing three critical challenges related to product characteristics, accuracy improvement algorithms, and operational implementation.
- This review provides comprehensive insights into the utilization of SPPs and reanalysis datasets for deriving reliable precipitation estimates in high-altitude regions.

Abstract

Accurate precipitation observation in high-altitude regions is of paramount importance for understanding climate variability and mitigating extreme hazards. However, obtaining reliable precipitation measurements in these areas remains a formidable challenge due to sparse gauge networks, complex topography, and intricate meteorological conditions. With the advent of remote sensing and numerical simulation techniques, satellite precipitation products (SPPs) and reanalysis datasets have emerged as effective alternatives to in-situ rain gauges. This review systematically examines the progress, challenges, and prospects of applying these precipitation products to address data scarcity, focusing specifically on high-altitude regions, with the Tibetan Plateau (TP) as the primary case study. The retrieval principles, advantages and limitations, applicability, and error characteristics of these products are first outlined. These precipitation products generally demonstrate significant conditional biases across multiple spatiotemporal scales and often lack the fidelity to accurately capture extreme events. Accordingly, the theoretical foundations, implementation procedures, and case studies of bias correction and product merging methods are analyzed to evaluate their potential for accuracy improvement in alpine regions. The results indicate that these methods have been effective in reducing errors in both precipitation estimates and hydrological simulations. Nevertheless, further efforts are needed to address key challenges related to the products themselves, the accuracy improvement

Check for updates

Academic Editor: Salvatore Manfreda

Received: 17 August 2026
Revised: 6 September 2026
Accepted: 9 September 2026
Published: 21 September 2026

algorithms, and their operational application. This review offers comprehensive guidance for leveraging SPPs and reanalysis datasets to obtain more reliable precipitation estimates in high-altitude regions.

Keywords: high-altitude regions; precipitation estimation; satellite precipitation products; reanalysis datasets; data scarcity

1. Introduction

Precipitation serves as a fundamental driver of the global water cycle and stands as the most active variable governing atmospheric circulation [1,2]. Its variability across diverse spatiotemporal scales dictates the complex interactions between the hydrosphere, atmosphere, and biosphere [3]. In high-altitude basins, precipitation exhibits pronounced spatiotemporal heterogeneity and complexity. Steep terrain forces lifting and cooling of moist air masses, leading to enhanced orographic precipitation on windward slopes and creating significant rain shadows on leeward sides [4]. This results in dramatic variations in precipitation amounts and phases over short distances. Consequently, precipitation in high-altitude regions is far more complex than in lowland areas, posing substantial challenges for accurate observation and monitoring.

Rain gauges provide relatively accurate point-scale observations of precipitation reaching the Earth's surface. However, the utility of gauge networks is significantly constrained by their uneven spatial distribution and inherent point-scale limitations [5,6]. First, gauge networks are severely sparse in high-altitude and remote areas. For example, although the China Meteorological Administration Multisource Precipitation Analysis (CMPA) comprises approximately 30,000 to 40,000 meteorological gauges across mainland China, only a tiny minority are located on the Tibetan Plateau (TP) [7]. The existing gauges are predominantly clustered in the eastern TP, leaving the western regions and the southern slopes severely sparse. Complex terrain, characterized by extreme elevations, steep slopes, and deep valleys, severely impedes site accessibility, infrastructure deployment, and long-term operational stability. Furthermore, gauge measurements represent only point-scale precipitation and cannot capture the spatial heterogeneity of precipitation around the gauge, particularly in topographically complex high-altitude areas where precipitation varies markedly over short distances [8]. Ground-based weather radars offer broader spatial coverage and can provide more continuous precipitation fields. However, their deployment is costly, and they are subject to terrain blockage, limiting their effectiveness in mountainous environments [9].

Although the scarcity of reliable in-situ meteorological observations remains a fundamental constraint in high-altitude basins, significant technological progress is mitigating this data gap. Progress in remote sensing capabilities and the increasing availability of satellite and numerical products provide alternative data sources. Satellite precipitation products (SPPs) retrieve precipitation estimates by interpreting signals from visible/infrared (VIS/IR) or microwave sensors aboard orbiting platforms, offering the advantage of quasi-global coverage and the ability to monitor precipitation over remote and inaccessible regions [10,11]. Reanalysis datasets, on the other hand, utilize data assimilation techniques to integrate multi-source observations with numerical weather prediction (NWP) models, producing physically consistent, long-term and spatiotemporally continuous records of atmospheric variables [12]. By presenting data on regular grids in both space and time, these gridded precipitation products are well suited for capturing the overall dynamics of precipitation and its localized characteristics, and are also readily integrable into hydrological models [13]. They have been widely applied in high-altitude regions, serving as a primary alternative source for precipitation estimation in gauge-scarce or ungauged regions. For example, near-real-time SPPs have proven valuable for extreme disaster prevention in high-altitude basins, enabling timely monitoring of intense precipitation events and supporting early warning systems for flash floods [14–16]. Reanalysis datasets have contributed significantly to climate research, enhancing the understanding of precipitation regime shifts under a changing climate over the TP and other alpine regions [17–19].

Despite their extensive utility, SPPs and reanalysis datasets are subject to various sources of error stemming from differences in retrieval algorithms, sensor characteristics, model parameterizations, and data assimilation schemes [10,20,21]. For SPPs, errors primarily arise from observation errors, sampling errors, and retrieval algorithm errors, among which algorithm errors originate from the indirect nature of the retrieval process [22]. VIS/IR sensors infer precipitation from cloud-top properties, while passive microwave sensors (PMW) rely on scattering and emission signals from hydrometeors, both of which are prone to misclassification and attenuation effects [23]. Topographic shading, surface snow cover, and complex terrain further degrade retrieval accuracy [24,25]. Reanalysis datasets inherit errors from the underlying forecast model, including deficiencies in convective parameterization, boundary layer processes, and orographic precipitation representation [13]. Therefore, prior to any applications of precipitation products in high-altitude regions, it is essential to conduct a thorough assessment of product applicability and implement appropriate bias correction or data fusion techniques to enhance their accuracy and reliability.

Single-product bias correction methods for SPPs and reanalysis datasets aim to reduce systematic biases by typically adjusting single products with ground-based gauge observations [12,14]. The underlying assumption is that gauge observations represent the "ground truth," and that error characteristics derived at gauge-located grid cells are transferable to gauge-free grid cells. By establishing the statistical relationship between gridded products and gauge observations at gauged locations, the correction scheme can then be extrapolated to ungauged areas to adjust the precipitation field. Commonly used approaches include conventional statistical methods, distribution-based approaches, and machine learning (ML) techniques. Beyond single-product bias correction, multi-source precipitation merging offers an alternative pathway for accuracy improvement by integrating the complementary strengths of different precipitation products, often yielding estimates superior to any individual product [26]. Multi-source fusion is particularly valuable when the accuracy improvement achieved by single-product bias correction remains insufficient. Depending on whether gauge observations are available during the merging process, these methods can be categorized into gauge-dependent approaches and gauge-independent approaches [21]. Both bias correction and product merging techniques have been proven to significantly improve the accuracy of precipitation estimates and hydrological performance [27–31]. Although previous studies have documented the application of SPPs and reanalysis datasets across various regions [3,10,13,32,33], many have primarily focused on evaluating and ranking selected precipitation products [34,35]. Systematic reviews that simultaneously examine product applicability, accuracy improvement methods, and key challenges specific to high-altitude environments remain scarce.

This paper provides a comprehensive overview of the application of SPPs and reanalysis datasets in high-altitude regions, critically reviewing current achievements, identifying potential challenges, and outlining future research directions. First, the concepts of SPPs and reanalysis datasets are introduced, including their precipitation retrieval principles and the attributes of commonly used products. Second, the inherent error sources, application advantages, and error performance of these products in precipitation estimation and hydrological simulation, primarily over a representative high-altitude region, the

https://doi.org/10.3390/hydrology13090259

TP, are examined. Third, the corresponding bias correction and product merging techniques developed for accuracy improvement in high-altitude regions are presented. Finally, the remaining product-related, algorithm-related, and application-related challenges are analyzed, and prospective recommendations for future research are discussed.

The remainder of this paper is organized as follows. In Section 2, the concepts of SPPs and reanalysis datasets are introduced. In Section 3, the applicability assessment of these gridded precipitation products in high-altitude basins is presented. Subsequently, the corresponding accuracy improvements are introduced in Section 4, and the potential challenges and future recommendations are discussed in Section 5.

2. Gridded Precipitation Products

2.1. Satellite Precipitation Products

Enabled by the convergence of space-based remote sensing, radiometer technology, and retrieval algorithms, SPPs have emerged as indispensable datasets for global hydrometeorology. Space-based remote sensing provides the essential platform for global observation, radiometer technology measures the physical radiance signals altered by hydrometeors, and retrieval algorithms transform these raw signals into quantitative precipitation estimates by solving complex inverse problems. Compared to ground-based gauges, satellite products offer spatially continuous and near-global coverage, effectively filling vast high-altitude areas [36,37].

Table 1 summarizes the basic information of major SPPs. The Tropical Rainfall Measuring Mission (TRMM) Multi-satellite Precipitation Analysis (TMPA) products, particularly 3B42 and 3B42RT, were among the most extensively applied datasets for hydrological and climatological studies, providing multi-satellite rainfall estimates across tropical and subtropical regions [38]. Following the conclusion of the TRMM mission, the Integrated Multi-satellitE Retrievals for Global Precipitation Measurement (IMERG) was introduced under the Global Precipitation Measurement (GPM) framework as the designated successor to TMPA [39]. Relative to its predecessor, IMERG provides broader spatial coverage, finer spatial and temporal resolution, and offers multiple latency options through its early, late, and final runs. Concurrently, other major satellite precipitation products have advanced along distinct methodological pathways. The Gauge-Adjusted Global Satellite Mapping of Precipitation (GSMaP-G) product integrates multi-satellite microwave and infrared observations with gauge information to produce gauge-calibrated rainfall estimates [40]. The Climate Prediction Center morphing technique (CMORPH) dataset utilizes motion vectors derived from geostationary (GEO) infrared imagery to propagate microwave-derived precipitation fields, followed by bias correction and optional gauge-based blending [41]. The Climate Hazards Group InfraRed Precipitation with Stations (CHIRPS) v3 product blends GEO thermal-infrared cold-cloud-duration estimates, a high-resolution precipitation climatology, and quality-controlled in-situ gauge observations through a variance-preserving, anomaly-based station-correction scheme [42]. The Precipitation Estimation from Remotely Sensed Information using Artificial Neural Networks (PERSIANN) family, including PERSIANN, PERSIANN-CCS, PERSIANN-CDR and PDIR-Now, represents another important lineage of algorithms based on artificial neural networks (ANNs) and cloud-classification techniques, with different products tailored to near-real-time monitoring, high-resolution estimation, and long-term climate analyses [43–45]. Collectively, these datasets illustrate a progression in satellite precipitation retrieval from early multi-satellite merging approaches toward higher-resolution, gauge-adjustable, and application-specific products, and have been widely utilized in high-altitude regions [37,46,47].

Table 1. Summary of basic information of major SPPs.

Product	Spatial Resolution	Finest Temporal Resolution	Coverage	Latency	Period	Reference
TRMM 3B42 v7	0.25°	3 h	50° S–50° N	/	31 December 1997–1 January 2020	[38]
TRMM 3B42RT v7			60° S–60° N		29 February 2000–2 January 2020	
IMERG-Early v7	0.1°	30 min	Global	~4 h	1998–present	[39]
IMERG-Late v7				~14 h		
IMERG-Final v7				~4 months		
GSMaP-Gauge	0.1°	1 h	60° S–60° N	~2–3 days	1998–present	[40]
CMORPH-BLD	8 km	30 min	60° S–60° N	/	1998–2019	[41]
CHIRPS v3	0.05°	1 day	60° S–60° N	Preliminary: ~2 days after each pentad; Final: ~3 weeks after month-end	1981–present	[42]
PERSIANN	0.25°	1 h	60° S–60° N	~2 days	1983–present	[45]
PERSIANN-CCS-CDR v2.0	0.04°	3 h	60° S–60° N	~3 months		[43]
PDIR-Now	0.04°	1 h	60° S–60° N	~15–60 min	March 2000–present	[44]

The retrieval of precipitation from space relies primarily on three distinct technologies [10,13,23], as shown in Figure 1: (1) VIS/IR sensors aboard both GEO and low Earth orbit (LEO) satellites, which estimate rainfall indirectly from cloud-top properties; (2) PMW sensors on LEO satellites, which provide a more direct physical measurement by detecting emission and scattering signals from hydrometeors; and (3) active microwave sensors (AMW) on LEO satellites, which offer the most direct and accurate measurement by actively probing the three-dimensional structure of precipitation. These three methodologies form the cornerstone of mainstream modern satellite-based quantitative precipitation estimation.

VIS/IR methods estimate precipitation indirectly by analyzing cloud properties derived from GEO and LEO satellites. The core principle is that cold and bright cloud tops are statistically associated with deep convection and a higher probability of rainfall [10,23]. Classic VIS/IR algorithms, such as the GEO Operational Environmental Satellites multispectral rainfall algorithm [48], are based on establishing empirical relationships between these cloud-top characteristics and surface rain rates.

Two prominent examples of VIS/IR-based precipitation products are Climate Hazards Group InfraRed Precipitation with Station data (CHIRPS) and PERSIANN. CHIRPS utilizes thermal infrared observations to derive a "cold cloud duration" index, which quantifies the persistence of cold cloud tops as a proxy for rainfall occurrence, and then heavily fuses this satellite information with in-situ gauge data to produce a bias-corrected, long-term climatological record [49]. PERSIANN primarily relies on infrared imagery from GEO satellites, employing ANNs to establish a complex statistical mapping between cloud-top brightness temperature patterns and surface rain rates [50]. However, the relationship between cloud-top properties and surface precipitation is indirect and non-unique, leading to potentially significant errors for warm-rain processes, cirrus clouds, and situations where precipitation occurs without pronounced cold cloud tops [10,23].

PMW radiometers on LEO satellites detect the natural microwave emission and scattering signals from precipitation-sized hydrometeors within clouds. Emission signals and scattering signatures have a quantifiable physical link to precipitation intensity. Advanced retrieval algorithms, such as the Goddard Profiling algorithm [51], solve this inverse problem to estimate instantaneous rainfall and its vertical structure. The key strength of

PMW retrieval compared to VIS/IR-based methods lies in its capability for all-weather, day-and-night detection and, more importantly, its direct sensitivity to precipitation-sized hydrometeors, which enables physically more robust estimation of surface rainfall [52,53]. Its main limitation is the relatively poor temporal sampling (~2–3 overpasses per day at a given location) from LEO platforms, which cannot capture the rapid evolution of precipitation systems as effectively as GEO-based IR [10].

AWM precipitation retrieval, primarily conducted by spaceborne precipitation radars, is recognized as one of the most accurate methods for measuring rainfall from space [54,55]. Exemplified by missions such as the Global Precipitation Measurement (GPM) [39] and China's Fengyun-3G (FY-3G) [56] series, the technique operates by actively transmitting a microwave pulse toward the Earth's surface and precisely measuring the power and characteristics of the signal backscattered by precipitation particles within the cloud. This allows for the direct retrieval of the three-dimensional structure, intensity, and type of precipitation [57]. However, its most significant limitation is the extremely narrow observational swath and sparse spatial coverage, which precludes its use for continuous, high-temporal-resolution monitoring on a global scale alone.

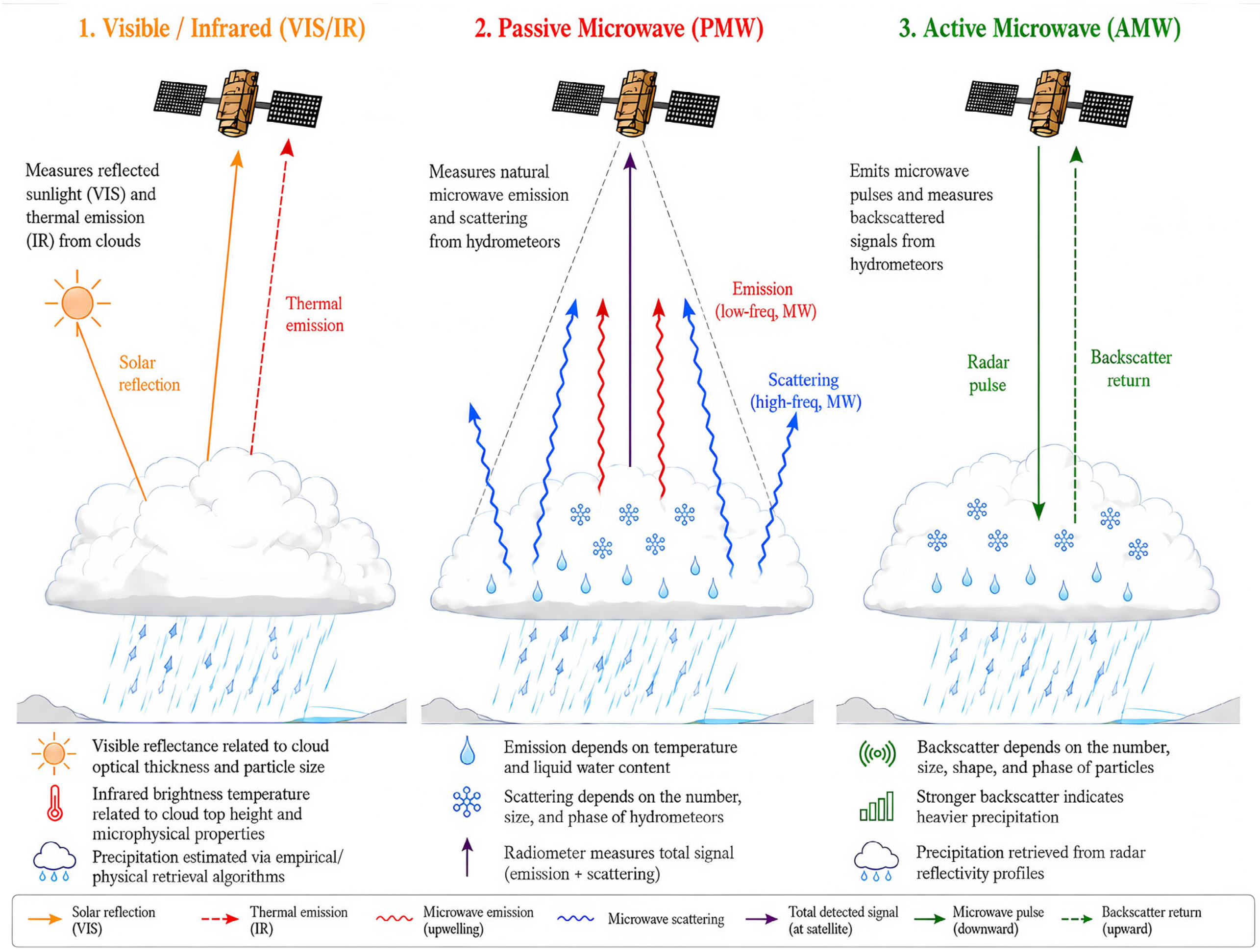

Figure 1. Illustration of satellite-based precipitation retrieval methods using visible/infrared (VIS/IR), passive microwave (PMW), and active microwave (AMW) sensors.

To overcome the limitations inherent in any single retrieval algorithm, the prevailing approach in satellite precipitation estimation has shifted toward the integration of multiple sensor types. This multi-sensor fusion paradigm strategically combines the high temporal continuity of GEO infrared observations, the direct physical sensitivity of PMW measurements, and the high-accuracy vertical profiling of AMW radars. For example, the GPM-IMERG [39] product unifies precipitation estimates by first intercalibrating all PMW sensors using active radar data as a physical benchmark. It then merges these calibrated PMW estimates with high-frequency GEO infrared imagery, using IR-derived motion vectors to interpolate rainfall between microwave overpasses, achieving a synthesis of PMW accuracy and IR continuity. The GSMaP [58] and CMORPH [41] first retrieve rainfall from multiple PMW sensors and then use IR-derived cloud motion vectors to propagate and interpolate these PMW estimates. While the GSMaP further applies a Kalman filter to blend the propagated PMW data with direct IR-based precipitation retrievals, the CMORPH relies on IR solely for feature advection via a morphing technique.

2.2. Reanalysis Products

Reanalysis datasets are generally categorized into global and regional products based on their spatial coverage. Global products are particularly valuable for providing continuous records in data-scarce regions and facilitating global climate assessments [59]. In contrast, regional products focus on specific target areas with higher spatial resolution, offering a more detailed representation of local atmospheric processes and topographical features [60]. Figure 2 presents a flowchart for reanalysis datasets. Table 2 summarizes the basic information of major reanalysis datasets.

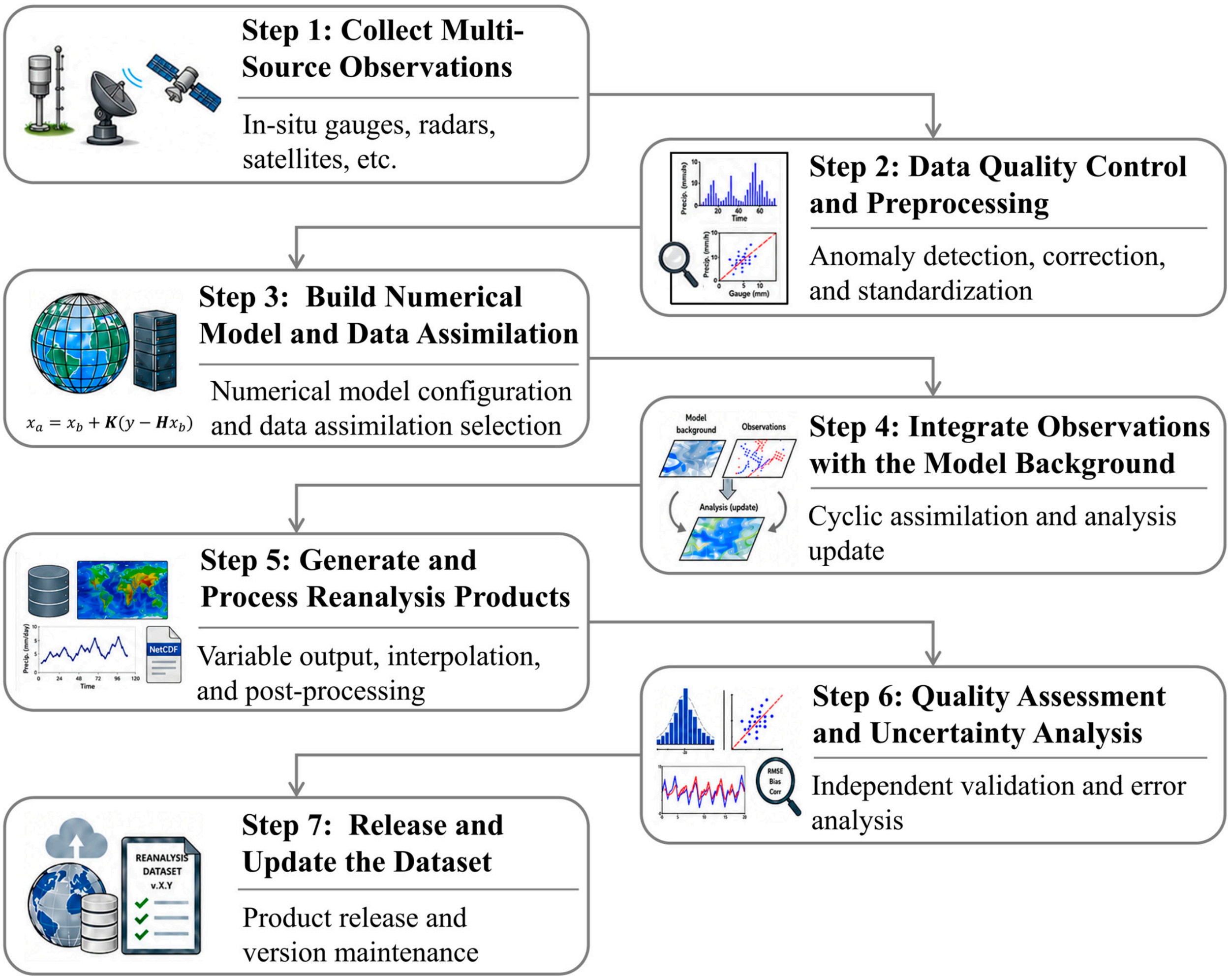

Figure 2. Flowchart for the generation of atmospheric reanalysis datasets.

Table 2. Summary of the basic information of reanalysis datasets.

Product	Spatial Resolution	Finest Temporal Resolution	Coverage	Latency	Period	Reference
Global reanalysis datasets						
ERA5	0.25°	1 h	Global	~5 days	1940–present	[61]
ERA5-Land	0.1°	1 h		~5 days	1950–present	[62]
GLDAS-2	0.25°	3 h	60° S–90° N	~3–4 months	1948–present	[63]
MERRA-2	0.5° × 0.625°	1 h	Global	~3 weeks	1980–present	[64]
JRA-55	1.25°	3 h	Global	Several days to weeks	1958–January 2024 (succeeded by JRA-3Q thereafter)	[65]
JRA-3Q	1.25°	3 h	Global	Several days to weeks	September 1947–present	[66]
NCEP2	2.5°	6 h	Global	Several days to weeks	1979–present	[67]
Regional reanalysis datasets						
NLDAS-2	0.125°	1 h	25° N–53° N, 125° W–67° W	~4 days	1979–present	[68]
CLDAS-V2.0	0.0625°	1 h	0° N–65° N, 60° E–160° E	~1 h/ 2 days	January 2017–present	[69]

The ERA5 is one of the most popular global atmospheric reanalyses produced by the European Centre for Medium-Range Weather Forecasts (ECMWF), which has replaced the ERA-Interim project [61]. ERA5 assimilates a wider range of satellite and in-situ observations using an advanced 4D-Var data assimilation system [70]. Key improvements include a significantly higher spatial resolution and hourly temporal resolution. ERA5-Land is produced by replaying the land component of the ECMWF NWP model, driven by the meteorological fields from ERA5 [62]. It offers an enhanced spatial resolution of approximately 9 km (0.1° × 0.1°), providing more detailed information on land surface variables such as soil moisture, snow depth, and vegetation water content, which are crucial for hydrological and agricultural applications.

The Global Land Data Assimilation System (GLDAS) was developed jointly by the National Aeronautics and Space Administration (NASA) and the National Oceanic and Atmospheric Administration (NOAA), with the first version released in the early 2000s [63]. Since its inception, GLDAS has undergone significant iteration, evolving from GLDAS-1 to the current GLDAS-2. The system employs advanced Land Surface Models (LSMs), such as CLM, Noah, and VIC, integrated with the Land Information System (LIS) framework to ingest satellite- and ground-based observational data, thereby producing optimal fields of land surface states and fluxes with a spatial resolution up to 0.25° [71].

The Modern-Era Retrospective analysis for Research and Applications, Version 2 (MERRA-2), is a global atmospheric reanalysis produced by NASA Global Modeling and Assimilation Office, officially released in 2015 to replace the original MERRA dataset [64]. MERRA-2 utilizes the GEOS-5 (Goddard Earth Observing System, Version 5) data assimilation system, which employs a 3D-Var analysis scheme with a Gridpoint Statistical Interpolation analysis to integrate a vast array of satellite and in-situ observations [64]. Compared with ERA5 and GLDAS, MERRA-2 has a coarser spatial resolution of 0.5° × 0.625°.

The JRA-55 is a global atmospheric reanalysis product developed by the Japan Meteorological Agency (JMA), spanning from 1958 onward (succeeded by JRA-3Q after

January 2024) [65]. It provides a comprehensive set of atmospheric, land surface, and diagnostic variables on a regular 1.25° × 1.25° latitude-longitude grid. Depending on the variable type, daily outputs are available at 3-, 6-, or 24-hourly temporal resolutions. As the successor to JRA-55, the Japanese Reanalysis for Three Quarters of a Century (JRA-3Q) extends the record back to September 1947 and incorporates major advances in JMA's data assimilation system, forecast model, boundary conditions, and historical observations [66]. JRA-3Q is continuously updated on a near-real-time basis and provides improved representations of precipitation and atmospheric variability relative to JRA-55.

The NCEP–DOE Reanalysis 2 (NCEP2), developed jointly by the National Centers for Environmental Prediction (NCEP) and the U.S. Department of Energy (DOE), represents a refined successor to the original NCEP/NCAR Reanalysis [67]. It incorporates corrections for previously identified processing errors and features updated model parameterizations. The dataset provides an extensive suite of atmospheric and surface variables on a global 2.5° × 2.5° grid, with most fields available at 6-hourly temporal resolution.

Regarding regional reanalysis datasets, the North American Land Data Assimilation System (NLDAS) is a collaborative project initiated in the late 1990s involving NOAA, NASA, and other U.S. research institutions [68]. The project has evolved through two major phases, NLDAS-1 and NLDAS-2, offering a high spatial resolution of approximately 0.125° and an hourly temporal resolution. A key advantage of NLDAS over global reanalysis products is its ability to provide highly detailed and spatially consistent land surface states specifically tailored for North American hydrological and meteorological applications, effectively minimizing uncertainties associated with coarse-resolution global models in this region [72,73].

The China Land Data Assimilation System V2.0 (CLDAS-V2.0) is a high-resolution meteorological forcing dataset developed and released by the China Meteorological Administration (CMA), specifically designed to focus on the Asian region (0–65° N, 60–160° E) [74]. This dataset provides high-quality atmospheric forcing data from January 2017 to the present, with a spatial resolution of 0.0625° × 0.0625° and an hourly temporal resolution. Compared to global reanalysis datasets, the distinct advantage of CLDAS-V2.0 lies in its dense assimilation of local automatic weather station observations across China, which significantly improves the accuracy of near-surface temperature, precipitation, and radiation estimates.

3. Applicability Assessment in High-Altitude Regions

3.1. Error Sources of SPPs and Reanalysis Datasets

Despite the remarkable advancements in SPPs, significant uncertainties persist due to discrepancies in retrieval algorithms and data fusion strategies, leading to biased estimates, particularly in high-altitude basins characterized by complex climatic and topographic conditions. These errors are primarily manifested as observation errors, sampling errors, and retrieval algorithm errors [22]. Specifically, observation errors arise from sensor calibration, instrumental noise, atmospheric interference, and limitations in discriminating precipitating from non-precipitating scenes, resulting in missed events and false alarms. Sampling errors arise from the discontinuous nature of satellite overpasses, where the revisit frequency and swath width fail to capture the strong intermittency and spatial variability of precipitation, particularly for short-duration convective events. Retrieval algorithm errors are induced by the inherent assumptions and physical constraints of the retrieval schemes, such as the inability of VIS/IR methods to operate at night or describe the non-unique relationship between cloud-top properties and surface rainfall. For VIS/IR retrievals, cloud-top properties are only indirectly related to surface rainfall, whereas PMW retrievals are affected by surface emissivity, precipitation microphysics, and phase discrimination. These limitations are amplified in high-altitude regions, where snow- and ice-covered surfaces can produce microwave scattering signatures similar to frozen hydrometeors, potentially generating false precipitation [75]. Consequently, SPP errors are strongly conditional on precipitation intensity, season, surface type, elevation, and terrain complexity [75–77]. In addition, multi-satellite merging and gauge adjustment introduce further uncertainties because differences among sensors, retrieval algorithms, temporal sampling, and the spatial representativeness of sparse gauge networks can be propagated into the final products [78,79].

Reanalysis datasets are affected by a different but equally complex set of uncertainties. Their accuracy is jointly influenced by the quality and temporal consistency of assimilated observations, the data-assimilation system, atmospheric model dynamics, and physical parameterizations [10,13,80]. Unlike directly assimilated atmospheric variables such as temperature and humidity, precipitation is largely generated by the model through parameterized cloud microphysics and convection, and modulated by moisture transport and land–atmosphere interactions, which results that precipitation suffers from more pronounced biases [81]. Furthermore, changes in assimilated observing systems, model configurations, and data availability over long reanalysis periods can introduce temporal inhomogeneities that complicate analyses of interannual variability and long-term trends [64,82]. Finally, uncertainties in gauge observations used either for validation or post-processing should not be regarded as negligible, particularly in high-altitude regions where wind-induced undercatch, snowfall measurement errors, and sparse gauge coverage may propagate into evaluation, bias correction, and merging procedures. Consequently, it is imperative to conduct a thorough applicability analysis and quantitative error assessment of SPPs and reanalysis datasets prior to their application in hydro-meteorological studies.

3.2. Evaluation Methods and Metrics

Applicability evaluation of precipitation products is commonly categorized into two methodological frameworks: direct and indirect assessments. The direct approach involves a "point-to-grid" comparison, where gauge observations are directly compared with the nearest grid cell of the precipitation product, thereby avoiding the introduction of spatial interpolation errors that can confound precipitation detection statistics [83]. Crucially, it mitigates terrain-induced uncertainties, as interpolating sparse gauge data across heterogeneous elevations can distort precipitation fields and artificially inflate the false alarm ratio, especially for marginal or no-rain events [84]. The evaluated products in the existing literature are predominantly post-processed and gauge-adjusted products. Conversely, the indirect approach evaluates products by using them as forcing data for the same hydrological models and comparing the resulting simulated streamflow against observed discharge. This method overcomes the spatial scale mismatch between point gauges and grid cells by assessing the integrated basin-wide precipitation signal [85].

Evaluation metrics for post-processed/gauge-adjusted products comprise categorical and continuous indicators. The former frequently assesses the accuracy of precipitation occurrence detection. Key metrics include the probability of detection (POD), the false alarm ratio (FAR), the false positive rate (FPR), the critical success index (CSI), and accuracy (ACC). POD quantifies the fraction of observed precipitation events correctly identified by the product, reflecting the model's effectiveness in capturing actual events. FAR measures the proportion of satellite-detected precipitation events that did not happen, highlighting the model's tendency for false alarm reporting. FPR quantifies the proportion of actual non-rainy events that are incorrectly classified as rainy. CSI integrates POD and FAR to provide a balanced measure of detection performance by accounting for hits, misses, and false alarms. Additionally, ACC represents the overall proportion of correct detections.

https://doi.org/10.3390/hydrology13090259

In contrast, continuous indicators evaluate the statistical consistency of the simulated precipitation or streamflow time series against gauge observations. The Pearson correlation coefficient (CC) quantifies the linear association between predicted and observed values. The mean absolute error (MAE) and root mean square error (RMSE) measure the average magnitude of prediction errors. The Nash–Sutcliffe Efficiency (NSE) and Kling–Gupta Efficiency (KGE) assess the overall goodness-of-fit of the time series. The relative bias (RB) evaluates the overestimation or underestimation of precipitation products, defined as the mean error normalized by the mean observed precipitation and expressed as a percentage. Table 3 summarizes these statistical metrics. Collectively, these metrics provide a comprehensive framework for validating satellite-based and reanalysis-based precipitation estimates.

Table 3. Summary of the statistical metrics used for precipitation product evaluation. *TPo*, FP, *FN*, and *TN* represent the counts of true positive events, false positive events, false negative events, and true negative events, respectively. S and O denote the simulated and observed values; T refers to the length of the simulated period, $\overline{O}$ is the average of observations, β refers to the ratio of simulated to observed mean values, r represents Pearson's correlation coefficient, and γ is the ratio of simulated to observed coefficients of variation. For satellite-based precipitation products, evaluation metrics are applied to post-processed/gauge-adjusted products.

Category	Metrics	Equation	Range	Perfect Value
Categorical	Probability of Detection (POD)	$\frac{TPo}{TPo+FN}$	[0, 1]	1
	False Alarm Ratio (FAR)	$\frac{FP}{TPo+FP}$		0
	False Positive Rate (FPR)	$\frac{FP}{FP+TN}$		0
	Critical Success Index (CSI)	$\frac{TPo}{TPo+FP+FN}$		1
	Accuracy (ACC)	$\frac{TPo+TN}{TPo+FP+FN+TN}$		1
Continuous	Pearson Correlation Coefficient (CC)	$\frac{\sum_{t=1}^{T}(S_t-\overline{S})(O_t-\overline{O})}{\sqrt{\sum_{t=1}^{T}(S_t-\overline{S})^2}\sqrt{\sum_{t=1}^{T}(O_t-\overline{O})^2}}$	$[-1, 1]$	1
	Mean Absolute Error (MAE)	$\frac{1}{T}\sum_{t=1}^{T}\lvert O_t - S_t\rvert$	$[0, +\infty)$	0
	Root Mean Square Error (RMSE)	$\sqrt{\frac{1}{T}\sum_{t=1}^{T}(O_t - S_t)^2}$	$[0, +\infty)$	0
	Nash–Sutcliffe Efficiency (NSE)	$1 - \frac{\sum_{t=1}^{T}(S_t-O_t)^2}{\sum_{t=1}^{T}(O_t-\overline{O})^2}$	$(-\infty, 1]$	1
	Kling–Gupta Efficiency (KGE)	$1 - \sqrt{(r-1)^2 + (\beta-1)^2 + (\gamma-1)^2}$	$(-\infty, 1]$	1
	Relative Bias (RB)	$\frac{S_t-O_t}{O_t} \times 100\%$	$(-\infty, +\infty)$	0

3.3. Performance of SPPs and Reanalysis Datasets over the Tibetan Plateau

3.3.1. Advantages

Taking the TP as the primary case study, previous studies have employed these methodologies and metrics to evaluate the applicability of precipitation products in high-altitude basins. Figure 3 presents the spatial distribution of rain gauges from the CMA and the Global Historical Climatology Network (GHCN) over the TP. The digital elevation model (DEM) used in Figure 3 was derived from the Shuttle Radar Topography Mission (SRTM) with a spatial resolution of 90 m [86]. Lyu et al. [34] highlighted the distinct advantages of SPPs in the relatively gauge-dense eastern TP, where IMERG-Final and GSMaP-Gauge demonstrated robust performance with CC of 0.71 and 0.70, and CSI values of 0.56 and 0.63, respectively. Conversely, ERA5 appears better suited for the central and western sectors of the plateau. In the Lower Yarlung Zangpo Basin, GSMaP_MVK_G, characterized by the lowest ordinary least squares MSE of 54.26 in the terrain-precipitation relationship, shows superiority in capturing the observed coupling between precipitation distribution and topographic features [15]. Furthermore, the appropriate selection of satellite and reanalysis precipitation products as hydrological model inputs can effectively support daily and monthly streamflow simulation, thereby helping to address the hydrological complexities characteristic of high-altitude basins [87,88].

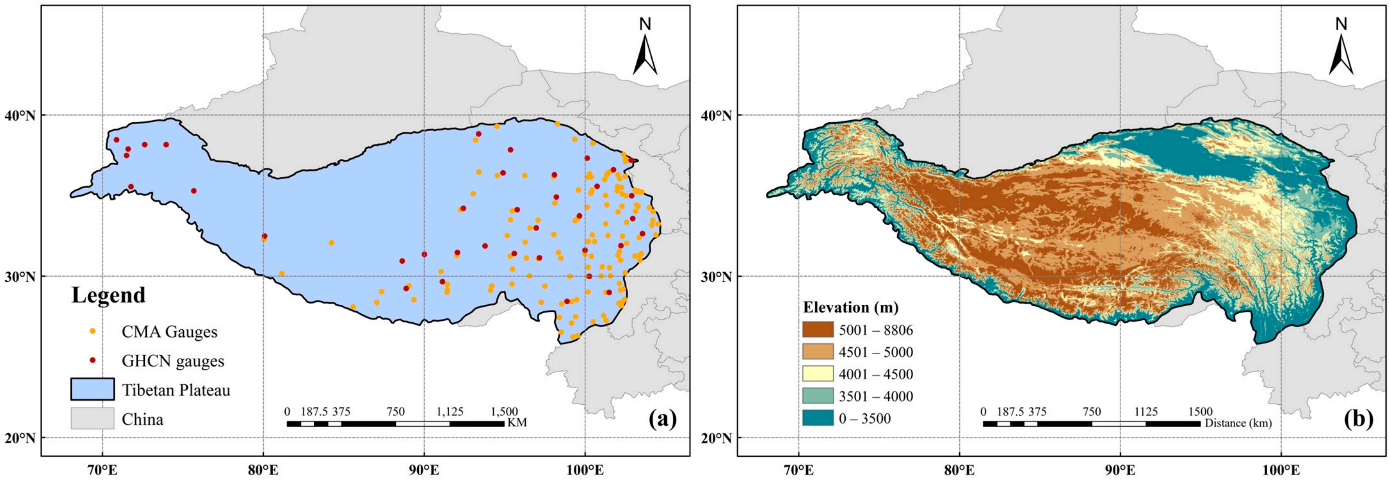

Figure 3. (**a**) Spatial distribution of rain gauges from the CMA and the GHCN over the TP; (**b**) topographic map of the TP.

Compared with SPPs, reanalysis datasets exhibit a superior capability to capture coherent spatiotemporal precipitation features across the TP [89–91]. From a spatial perspective, reanalysis data exhibit high spatial correlation with gauge measurements. For instance, over the eastern periphery of the TP, ERA5 precipitation demonstrates spatial correlation coefficients exceeding 0.8 in representing the evolution of regional rainfall events [92]. In terms of temporal characteristics, reanalysis products are more effective at longer time scales, successfully reproducing the interannual and decadal variabilities of precipitation. These combined spatial and temporal advantages render reanalysis data a particularly valuable resource for precipitation-related studies in high-altitude regions [89,93]. ERA5 is also recommended for hydrological modeling in High Mountain Asia, owing to its capacity to represent orographic gradients and its consistency in simulating observed streamflow [94]. GLDAS exhibits complementary strengths with ERA5 in describing precipitation over the TP. GLDAS performs well in representing the occurrence frequency of daily precipitation, but struggles to precisely detect individual daily precipitation events [89]. Conversely, ERA5 demonstrates a strong capability in detecting but tends to overestimate the frequency of daily precipitation [89]. This complementary behavior suggests that different reanalysis products capture different aspects of the precipitation regime.

3.3.2. Errors

However, despite these encouraging results, the application of SPPs in high-altitude regions is still constrained by non-negligible errors. Spatially, retrieval accuracy exhibits significant heterogeneity. Figure 4 shows the spatial distribution of CC, RMSE, and RB for four major SPPs at the monthly scale over the TP. The performance is generally superior in the eastern regions, and declines notably in the interior and high-elevation zones [16,77]. This degradation is largely attributed to the complex topography and heterogeneous land surface conditions [95]. Seasonally, products demonstrate higher accuracy during the warm season, whereas performance deteriorates in winter [77]. Figure 5 presents the seasonal evaluation of precipitation datasets over the TP. The winter season, characterized by frequent light and solid precipitation, is associated with reduced correlation coefficients and an increased rate of false alarms [95,96]. At the daily scale, IMERG tends to underestimate the frequency of light-to-moderate rainfall while overestimating the occurrence of torrential and extreme events [97]. At the hourly scale, the product underestimates precipitation amounts from the early morning to midday but overestimates them from the afternoon through late night [97]. Furthermore, as shown in Figure 6, a consistent bias is observed across multiple datasets, which exhibit a tendency to overestimate low precipitation rates and underestimate high-intensity events [34,77,98,99]. This phenomenon is probably attributed to the limited sensitivity of satellite sensors to light precipitation [100].

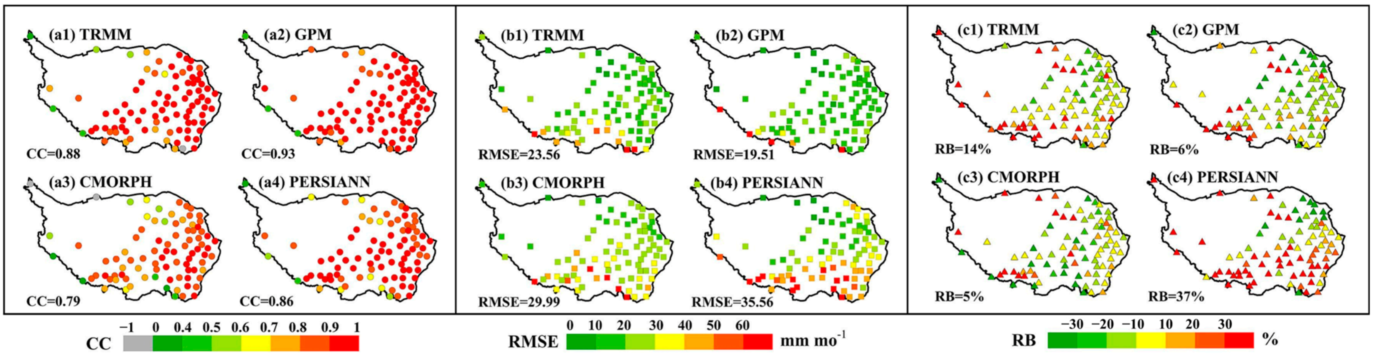

Figure 4. Spatial distribution of CC, RMSE, and RB for four major SPPs at monthly scale over the TP. Reproduced from [35]. The red, green, and yellow indicate the best performance for CC, RMSE, and RB, respectively.

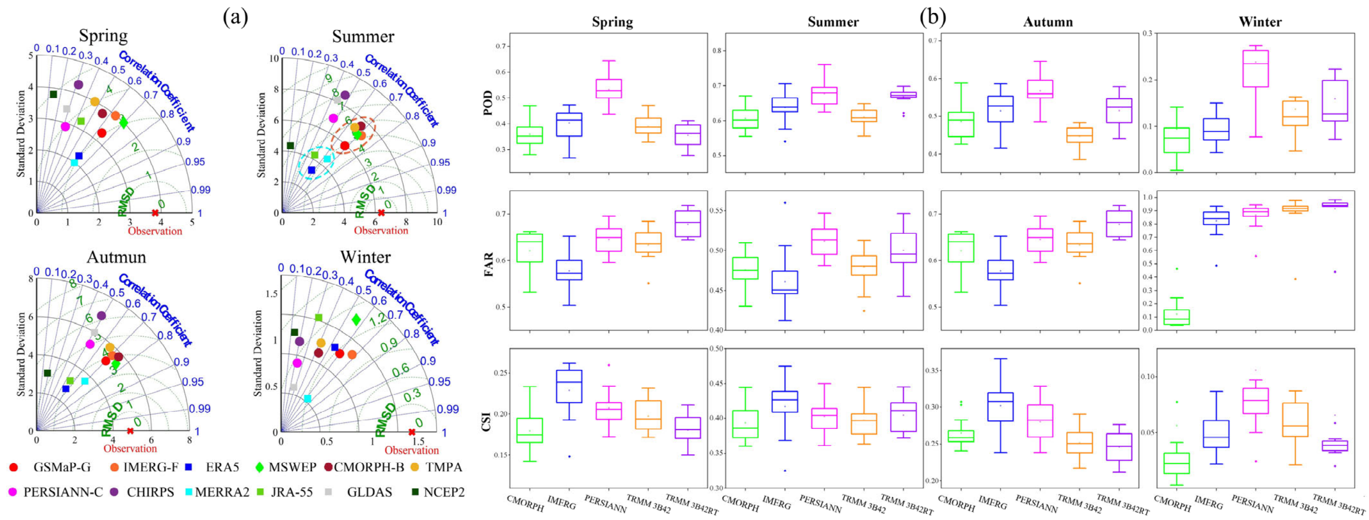

Figure 5. Seasonal evaluation of precipitation datasets over the TP. (**a**) Continuous metrics shown via Taylor diagrams for twelve precipitation datasets at the daily scale. The red cross on the *X*-axis denotes gauge observations. Reproduced from [34]. (**b**) Boxplots of categorical metrics for five SPPs evaluating daily extreme precipitation events exceeding the 75th percentile of all rainy days. Reproduced from [77].

Evidence from high-elevation regions beyond the TP can further deepen our understanding of these biases. Similar error patterns have been reported over mountainous regions such as the Himalayas, the Peruvian and Colombian Andes, the Alps, and the Lake Titicaca region [75,76]. SPPs commonly exhibit rain-rate-dependent biases, with light precipitation tending to be overestimated and heavy precipitation underestimated, partly because of false detection of weak rainfall and insufficient sensitivity to shallow orographic warm-rain processes [75]. Their performance is also strongly elevation dependent. In some cases, SPPs fail to reproduce observed precipitation-elevation gradients or show larger missed-rainfall and false alarm errors at higher elevations [75]. Surface conditions introduce additional biases, as snow- and ice-covered land can generate microwave scattering signatures similar to those of frozen hydrometeors and thus cause spurious precipitation, whereas warm-cloud precipitation over mountainous areas or high-altitude lakes may be missed [76]. These errors are also scale dependent. Daily and point-to-grid evaluations tend to expose event-timing errors, spatial displacement, and point-to-area representativeness mismatches more directly, whereas temporal or basin-scale aggregation can partially cancel or smooth these discrepancies [75]. Although gauge adjustment can reduce some systematic and random errors, its effectiveness is not universal and may remain limited or even deteriorate at high elevations when the gauge information used for calibration is spatially unrepresentative [75,76].

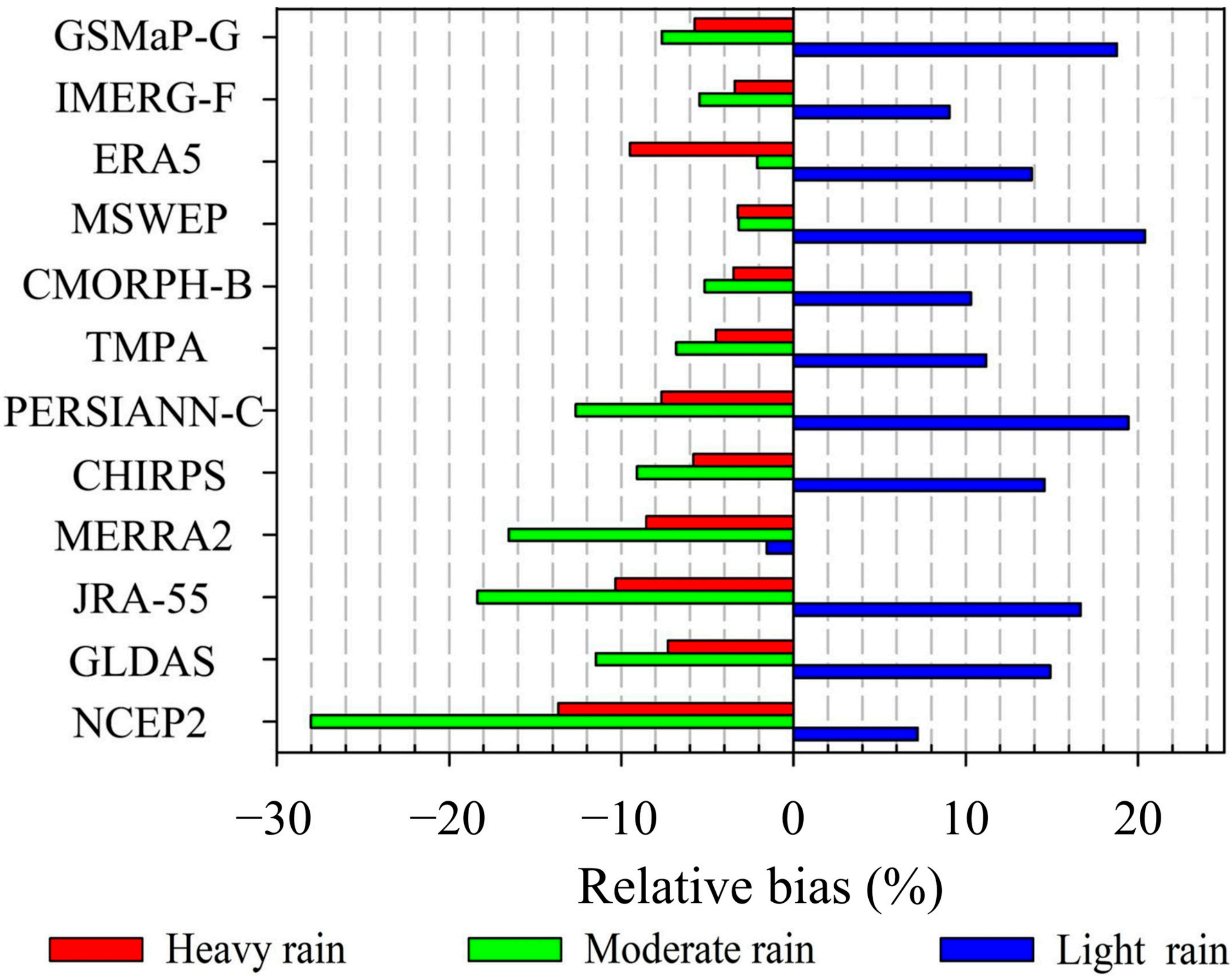

Figure 6. Comparison of histograms showing the relative bias of precipitation datasets against the gauge-based product CMPA across three rain intensity categories over the TP: heavy (>50 mm/day), moderate (5–50 mm/day), and light (0.1–5 mm/day). Reproduced from [34].

When hydrological models are employed to indirectly evaluate SPPs, the simulated streamflow also inevitably contains some inherent biases. Zhang et al. [101] conducted a hydrology-based indirect assessment of four gridded precipitation datasets, revealing that IMERG Final Run Version 06 still induces notable biases in flood simulations. This finding is also observed in Figure 7b,c, where deviations in simulated peak flows forced by IMERG-E and IMERG-F are evident in the upper Yellow River basin [91]. Therefore, given the inherent errors in satellite-based precipitation estimates, continuous efforts toward accuracy enhancement are essential.

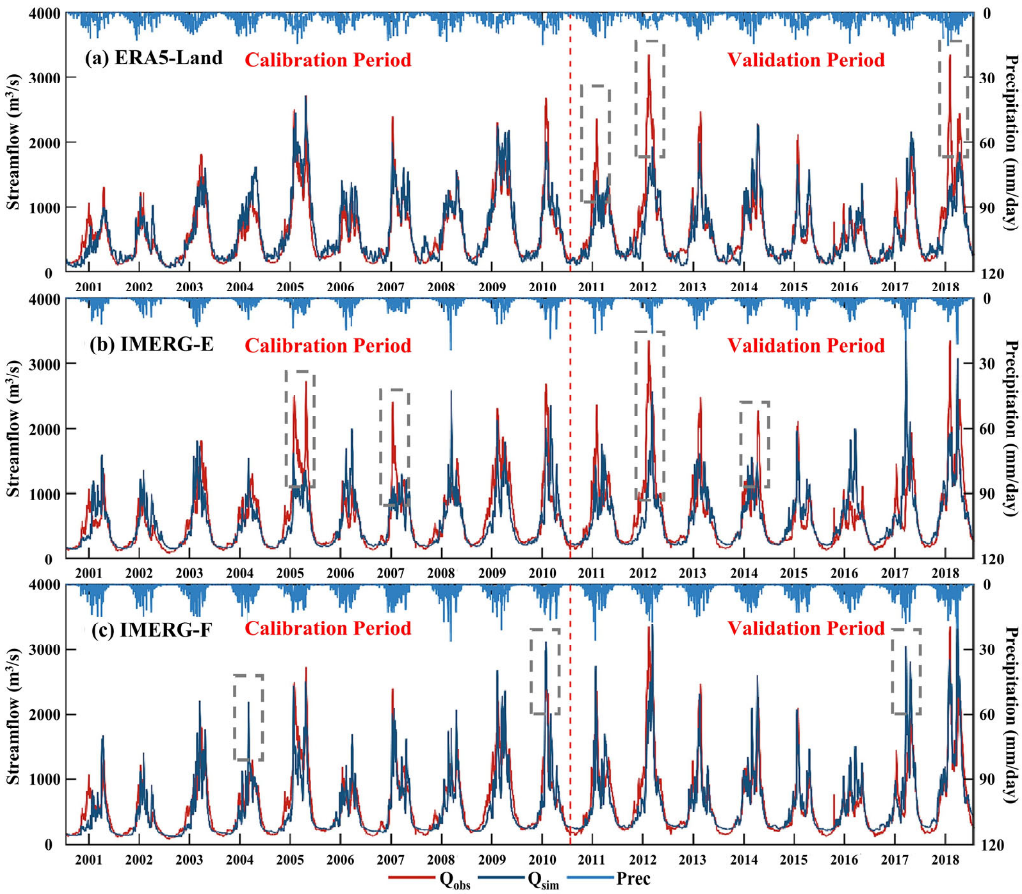

Figure 7. Comparison between observed and simulated daily streamflow forced by (**a**) ERA5-Land, (**b**) IMERG-E, and (**c**) IMERG-F. The gray dashed boxes indicate the deviated peak flow simulations. Modified from [91].

Similar to SPPs, reanalysis datasets suffer from notable biases in TP as well. First, they tend to overestimate the overall precipitation amount [94,102]. For example, Figure 8a shows the overall precipitation overestimation of ERA5-Land. Meanwhile, Figure 8b demonstrates that the monthly mean precipitation derived from ERA5-Land is roughly twice the observed precipitation for nearly all months, with a particularly pronounced overestimation during the cold season [91], owing to high wind speeds and excessive external water vapor as represented in climate model simulations [35]. In contrast, IMERG-F exhibits relatively better performance in capturing the monthly mean precipitation.

Furthermore, regarding precipitation intensity, reanalysis datasets exhibit a consistent systematic bias, similar to that observed in SPPs, to overestimate low precipitation rates while underestimating high precipitation ones (Figure 6) [34,99]. ERA5 family also tends to overestimate the occurrence frequency of precipitation [89,91]. The overestimation of low- to intermediate-intensity precipitation events is probably attributed to atmospheric models with a cumulus parameterization scheme, which tends to release convective instability too readily and thereby results in overly frequent triggering of convection [92,103,104]. Seasonally, the overall performance of reanalysis datasets is inferior to that of SPPs during summer, when precipitation is more concentrated [99,105]. This seasonal limitation suggests that the ERA5 family struggles to accurately capture the variability of the monsoon-dominated precipitation regime over the plateau.

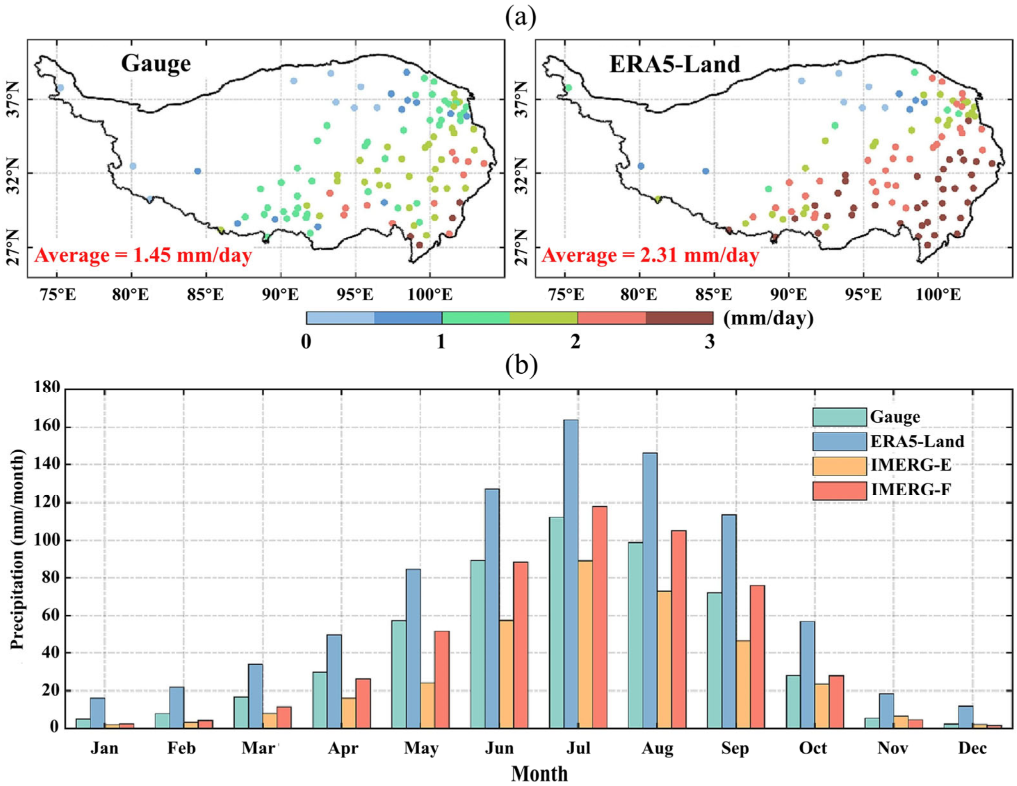

Figure 8. Comparison of precipitation amounts with gauge observations at daily and monthly scales over the TP during 2001–2018. (**a**) Spatial distribution of daily mean precipitation of the gauge observations and ERA5-Land. (**b**) Mean monthly precipitation of gauge observations and the three selected precipitation products at their corresponding grids. Reproduced from [91].

Regarding hydrological performance, reanalysis data are generally unable to adequately extract the extreme runoff patterns and underestimate peak flows, as observed in the source regions of the Yellow River and the Yangtze River [87]. Figure 7a reveals an underestimation of peak flows when evaluating the hydrological performance of ERA5-Land in the upper Yellow River basin. Moreover, the ability of reanalysis datasets to represent local trends at hydrologically relevant scales remains region dependent. Evidence from Mediterranean orographic regions shows that products such as ERA5 may capture the overall direction of variability while smoothing or missing locally pronounced trends observed by dense gauge networks, particularly in areas of complex topography [106].

4. Accuracy Improvement of Precipitation Products

To obtain a reliable and precise precipitation field, accuracy improvement techniques need to be applied to precipitation products before directly employing them in high-altitude regions. Figure 9 presents the classification of these techniques, which can be broadly grouped into two categories: single-product bias correction and product merging. Table 4 presents a comparative assessment of accuracy improvement methods for precipitation products.

Single-product bias correction refers to the statistical adjustment of single satellite-based or reanalysis-based precipitation estimates using reference gauge observations to reduce systematic errors and produce more accurate gridded precipitation fields [12,14]. It mainly includes conventional statistical, distribution-based, and ML-based approaches. Meanwhile, multiple precipitation product merging represents another promising pathway for improving precipitation estimation accuracy. This strategy holds particular promise for areas where single-product bias correction remains inadequate. Product merging methods can be further classified into gauge-dependent and gauge-independent approaches [21]. While bias correction typically enhances the precision of a single precipitation product, fusion techniques integrate the complementary strengths of multiple precipitation sources to reduce errors, thereby generally outperforming any individual contributing product [26]. These two methodological frameworks are reviewed in detail in the following sections.

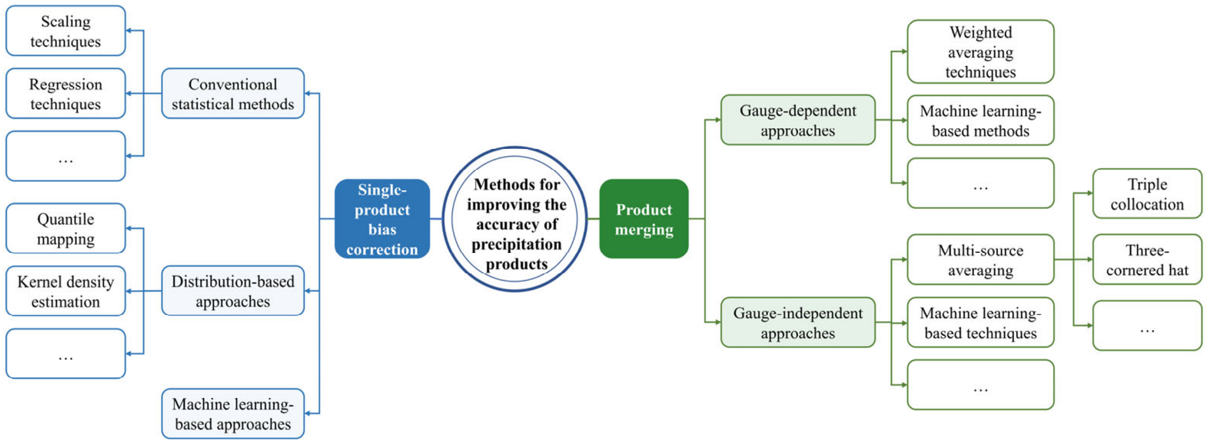

Figure 9. Classification of precipitation product improvement methods.

Table 4. Comparative assessment of accuracy improvement methods for precipitation products.

Category	Method	Advantages	Limitations	Expected Suitable Contexts
Single-product bias correction	Conventional statistical methods	Simple, transparent, computationally efficient; effective for stable systematic bias	Limited ability to capture temporal variability and non-stationary biases; may introduce interpolation uncertainty in data-sparse regions	Best suited to regions with relatively stable bias relationships and sufficient gauge observations
	Distribution-based methods	Correct precipitation distributions and quantiles; better represent frequency and variability	Sensitive to temporal structure, transformation assumptions, and reference-data representativeness	Have reliable and representative gauges; applications emphasizing distributions, variability, and quantiles
	Machine learning methods	Capture inherently complex, nonlinear, and spatially varying errors; can integrate multi-source auxiliary variables	Data-intensive; risk of overfitting; limited interpretability and transferability	Complex terrain with sufficient training data and auxiliary predictors
Product merging	Gauge-dependent approaches	Effectively exploits complementary strengths of multiple products and reduces merging uncertainties through gauge information	Depends on gauge density and representativeness; sparse networks and gauge sampling errors can limit merging performance	Single-product bias correction remains inadequate
	Gauge-independent approaches	Do not require gauges for merging; useful in data-scarce regions and can combine complementary satellite, reanalysis, or model information	May rely on assumptions about product independence or transferability; biased or correlated inputs can degrade the merged result	Best in poorly gauged or ungauged regions where multiple reasonably independent and complementary products are available

4.1. Single-Product Bias Correction

Generally, single-product bias correction consists of a two-step process. First, at locations where rain gauges are present, the error patterns of the precipitation products are diagnosed by treating gauge observations as references. Second, these diagnosed error patterns are employed in gauge-free grid cells to correct product errors, facilitating the adjustment of the entire precipitation field.

Specifically, the single-product bias correction methods are broadly categorized into three approaches. The first approach is conventional statistical methods, representing the fundamental techniques for bias correction by utilizing discrepancies between satellite-estimated and gauge-observed precipitation [107–109]. These methods are simple, computationally efficient, and effective for correcting stable systematic biases. They primarily include scaling techniques and regression techniques. Scaling methods, such as linear scaling, are widely adopted for their simplicity and robustness. They directly employ rain gauge data to remove the mean bias of precipitation products at daily or monthly scales, effectively adjusting the long-term average precipitation amount [110,111]. Regression methods adjust biases by establishing statistical relationships between satellite estimates and other covariates. For instance, techniques like stepwise regression (STEP) and geographically weighted regression (GWR) tune the spatial patterns of model parameters related to rainfall occurrence and intensity [46,112]. Lu et al. [46] employed the STEP and GWR to correct the bias of the downscaled IMERG precipitation dataset over the Tianshan Mountains, and the results showed that the correction effect becomes more pronounced as the altitude increases. Despite their widespread use, these conventional statistical methods possess notable limitations, particularly when applied to sparsely gauged areas such as high-altitude basins. Scaling methods often fail to capture temporal variability and higher-order moments [113,114]. Moreover, the underlying assumption of a stationary relationship between observed and numerically modeled data may not be applicable in response to climate change [31]. Similarly, while regression techniques can integrate sparse records, they struggle to adjust biases in the timing of events in real-time and introduce additional uncertainties through interpolation in data-scarce regions [111,115]. Therefore, conventional statistical methods are suited to regions with relatively stable bias relationships and sufficient gauge observations, particularly when correcting systematic mean biases rather than event timing or complex non-stationary errors.

The second category of bias correction methods is distribution-based approaches, which aim to align the probability distribution of satellite-derived or reanalysis precipitation estimates with that of reference observations [113,116]. Compared to conventional statistical methods that merely correct mean biases or linear relationships, distribution-based techniques represent better frequency and variability, and offer greater adaptability. They are suited to regions with representative gauge records where correcting precipitation distributions and quantiles is the primary objective. Commonly employed distribution-based methods include quantile mapping (QM), Gaussian anamorphosis (GA), and kernel density estimation (KDE). QM adjusts the bias of precipitation products by matching the quantiles of the modeled distribution to those derived from ground-based observations, thereby correcting the mean, variance, and higher-order moments of the precipitation distribution simultaneously. It has been widely recognized as an effective approach for reducing systematic biases in remotely sensed precipitation estimates [117–119]. However, it fails to adjust the temporal structure of precipitation, leading to inaccurate depiction of wet and dry spell durations [111]. To explicitly consider orographic characteristics of high-altitude regions, Velasquez et al. [120] introduced a preliminary step that differentiates orographic features based on elevation and slope orientations prior to applying empirical QM for bias correction. Besharatifar et al. [121] incorporated orographic effects into Quantile-QM, which provides more precise precipitation estimates in areas with substantial elevation gradients compared to traditional methods. For GA methods, it transforms non-normally distributed precipitation data into a Gaussian space, where standard bias correction techniques can be applied before transforming back to the original space, though its performance depends heavily on the appropriateness of the transformation function [122]. Alternatively, KDE provides a non-parametric pathway by estimating the probability density functions of both observed and simulated precipitation without assuming a predefined distributional form, offering greater flexibility at the cost of increased computational demand and sensitivity to bandwidth selection [123]. Collectively, while distribution-based methods represent a substantial improvement over traditional statistical approaches, their effectiveness in complex terrain regions with sparse gauge networks still remains constrained by the representativeness of the reference observations used to construct the target distributions.

The third category of bias correction methods is ML-based approaches, which have emerged as a promising alternative to traditional bias correction approaches in recent years [124–126]. Compared to conventional statistical and distribution-based methods, ML techniques offer distinct advantages by capturing inherently complex and nonlinear relationships between satellite-derived variables and ground-based observations, achieving better results in topographically intricate areas [127–129]. These models can integrate multi-source auxiliary variables without imposing explicit assumptions about data distributions, thereby providing greater flexibility and adaptability to quantify uncertainty in bias-corrected estimates [130]. They are suitable for complex terrain when sufficient training data and auxiliary predictors are available. The three most commonly employed ML models are random forest (RF), XGBoost, and long short-term memory (LSTM) networks. RF operates by constructing an ensemble of decision trees and aggregating their predictions, effectively handling high-dimensional input spaces and capturing nonlinear interactions while being relatively robust to overfitting [131]. XGBoost, a gradient boosting framework, builds trees sequentially by minimizing a loss function, offering improved predictive accuracy and computational efficiency through regularization and parallel processing [132]. With the advent of increased computational power, deep learning (DL) methods have become a promising avenue owing to their strong capacity for extracting spatiotemporal features. LSTM networks, one of the most representative DL models, are architecturally tailored for handling sequential data and utilize gating mechanisms to capture temporal correlations [133]. Wang et al. [134] developed a terrain-aware XGBoost network, which incorporates detailed physical topographic factors including elevation, slope, and trigonometrically decomposed aspect as auxiliary features. The network succeeds in extracting the physical modulation mechanisms of complicated terrain on local precipitation of the TP. Sambyal et al. [31] compared the four statistical approaches and four ML bias correction methods of ERA5-Land precipitation in the North Western Himalayas, and found that RF achieved the best accuracy. However, significant limitations of ML techniques include their limited physical interpretability and relatively large data requirements [111,135].

Regardless of the bias correction approach employed, the quality of the corrected precipitation estimates is fundamentally constrained by the spatial distribution and density of gauge stations. All these methods rely, to varying degrees, on reference observations to establish correction relationships, meaning that sparse and unevenly distributed gauge networks inevitably limit the reliability of bias-adjusted outputs. This issue poses a persistent challenge, particularly in high-altitude basins characterized by complex terrain and sparse monitoring networks.

4.2. Product Merging

4.2.1. Gauge-Dependent Approaches

Gauge-dependent approaches can be further divided into two types. By using gauge observations to optimize merging weights or train nonlinear fusion models, the merging uncertainties can be reduced through gauge information, and the complementary strengths of different precipitation products can be effectively exploited. The first type comprises weighted averaging techniques. Its underlying principle is to first utilize gauge measurements as references to evaluate the error characteristics of each individual precipitation product. Based on the assessed error metrics, fusion weights are then assigned to each product accordingly, with smaller errors assigned larger weights. The final fused precipitation estimate at each grid cell is subsequently obtained as a weighted combination of the individual products. The Multi-Source Weighted-Ensemble Precipitation (MSWEP) dataset is a representative example [136]. MSWEP merges rain gauge measurements, satellite estimates, and reanalysis datasets as a function of both timescale and location [10,136]. Specifically, the weight allocated to gauge measurements is determined by the local gauge network density, while the weights assigned to the other two candidates are derived from their comparison against surrounding gauge observations. Bayesian model averaging (BMA) is another widely employed technique [137]. It constructs a probabilistic forecast by computing a weighted average of candidate products, where the weights are derived from the historical performance of each product against ground-based gauge observations. By assigning higher probabilities to more accurate sources and accounting for the conditional probability density of the observations, BMA effectively synthesizes the strengths of individual datasets to produce a fused product with reduced uncertainty and improved reliability [138]. Ma et al. [139] followed a two-stage "bias correction-merging" fusion approach using BMA, and found that even in heavy rainfall events, the merged dataset still demonstrates significant improvement in the northeastern TP.

The second type of gauge-based approaches is ML-based fusion methods. These methods treat precipitation estimates from various products at grid points as input features, while using gauge-measured precipitation as benchmark labels. By training algorithms on these paired datasets, the model automatically determines how to optimally combine information from multi-source estimate products, effectively correcting systematic errors and generating a fused precipitation product with superior accuracy [140]. Nan et al. [30] utilized an ANN algorithm and a convolutional neural network (CNN) algorithm to realize the fusion of multi-source precipitation data, including CN05.1, IMERG, and a set of ERA5 dynamic downscaling datasets. Results show that the fusion of the products reduces the error and greatly improves the precipitation detection capability over the TP. Furthermore, the results exhibit better hydrological performance. Zhao et al. [141] involved seasonal precipitation characteristics and terrain factors into a ML framework, which largely enhanced the precise of the precipitation product in the high-altitude Yalong River Basin, with CC increasing from 0.52 to 0.84 and RMSE reducing from 5.5 mm/day to 1.99 mm/day.

The China Meteorological Forcing Dataset (CMFD) is a representative merged near-surface meteorological dataset, which is constructed by fusing ground-based observations from the CMA and NOAA with multiple gridded datasets, including GLDAS, MERRA, and TRMM [142]. It has a three-hourly temporal resolution and a 0.1° spatial resolution. The latest version CMFD v2.0 expands its data sources to ERA5, ISCCP-ITP-CNN and TPHiPr dataset, and transitions its production framework toward ML techniques. It stands out as one of the most precise products for reproducing precipitation patterns and streamflow characteristics over the TP across multiple intensities and spatiotemporal scales, compared to other mainstream SPPs and reanalysis datasets [87,99,143].

However, gauge-dependent merging approaches still rely on gauge precipitation observations and inevitably suffer from challenges analogous to those encountered by bias correction approaches. In high-altitude regions, the potential for accuracy improvement remains restricted by the spatial distribution of sparse monitoring networks and the sampling errors inherited in gauge measurements [13,144]. Therefore, these approaches are more effective in regions with sufficiently representative and reliable gauge observations.

4.2.2. Gauge-Independent Approaches

To address this challenge, gauge-independent fusion methods have been developed, which leverage the intrinsic characteristics and cross-comparisons among multiple satellite and reanalysis products to derive an optimized merged product without relying on in-situ gauge observations [145]. They are suitable in poorly gauged or ungauged regions where multiple reasonably independent and complementary products are available. Common gauge-independent fusion methods include multi-source averaging and ML techniques.

Multi-Source Averaging

Triple Collocation (TC) is one of the most representative methods of multi-source averaging [21,146]. The fundamental assumption of TC is that the errors among the three mutually independent precipitation products are uncorrelated, allowing the error variances of each product to be estimated solely from their pairwise covariances [147]. Under this framework, the method analyzes the statistical relationships between three independent estimates of the same precipitation variable to quantify the relative accuracy of each product without requiring an external reference. Once the error variances are derived, fusion weights are assigned inversely proportional to these estimated errors. Wu et al. [148] systematically examined the effectiveness of TC for multiple SPPs fusion over TP. The TC approach outperformed the individual SPPs and largely reduced the relative bias, exhibiting its reliability for merging SPPs in ungauged regions.

However, TC is subject to several important limitations. First, it is fundamentally designed to handle only random errors and cannot account for common systematic biases shared among the datasets. For example, SPPs tend to overestimate low-intensity events and underestimate high precipitation rates [34,77]. This systematic bias will remain uncorrected in the fused estimate, as TC treats it as part of the signal rather than an error. Second, the method relies on the critical assumption that errors among the three datasets are mutually uncorrelated. In practice, however, this assumption is sometimes violated, as some SPPs share common input data sources or algorithms [149,150]. These limitations collectively hinder the effectiveness of TC in accurately estimating precipitation and, consequently, in supporting hydrological simulation [151].

The Extended Triple Collocation (ETC) framework introduces a significant improvement by additionally estimating the error correlation coefficient between each individual product and the unknown true signal [152]. It leverages inter-product covariance structures to characterize relative product skill and relaxes the practical constraint of perfectly uncorrelated biases, providing a more flexible framework for gauge-independent precipitation fusion. Wei et al. [153] integrated the ETC and cumulative distribution function to blend SM2RAIN-ASCAT, IMERG Early Run, and the Climate Prediction Center (CPC) global unified gauge-based products. The ETC yields more robust performance than TC in determining the optimal weight for each collocated estimate.

As another alternative to TC, signal-to-noise ratio optimization (SNR-opt) constructs a noise-to-signal ratio matrix from the empirical covariance of the input datasets, quantifying each product's random error relative to the true signal [26,27]. Products with lower noise-to-signal ratios receive larger weights. Unlike TC, SNR-opt does not require zero error cross-correlation or a unit-sum constraint on weights. Shah et al. [27] introduced the SNR-opt framework to blend precipitation products in the Himalayas. This framework has the flexibility of estimating both low and heavy precipitation and reduces the bias for extreme rainfall.

ML Techniques

Similar to their prominent role in gauge-dependent fusion methods, ML techniques have also assumed an important position in gauge-independent approaches. Distinct from multi-source averaging, they automatically learn optimal fusion strategies from data, without requiring explicit assumptions about error distributions or product independence. Beyond the gridded precipitation products themselves, ML methods can also incorporate a variety of precipitation-related environmental variables as additional predictors to enhance the accuracy of the fused precipitation estimates. Input features, involving topographic factors, normalized difference vegetation index (NDVI), surface temperature, and seasonal characteristics, are proven to contribute to the accuracy improvement of merged precipitation datasets [141,154–156].

DL offers the distinct advantage of autonomously extracting hierarchical spatiotemporal features from high-dimensional and heterogeneous input data. By replacing the fully connected feed-forward connections between layers with convolutional structures, the convolutional long short-term memory (ConvLSTM) retains the temporal modeling capability of LSTM while simultaneously acquiring the ability to describe local spatial features [157]. This unique architecture makes ConvLSTM particularly well suited for capturing the spatiotemporal characteristics of precipitation fields, and has been proven effective in high-altitude complex terrain regions [158]. As another state-of-the-art DL architecture, Transformer represents a paradigm shift in sequence modeling by discarding recurrent structures, relying exclusively on self-attention to weigh the significance of different input parts dynamically [159]. Its structure has a benefit for capturing non-local precipitation patterns and dependencies that span large geographical distances, and overcomes the limited receptive fields and sequential processing bottlenecks inherent in traditional CNN and RNN-based methods. Microsoft's atmospheric foundation model, Aurora, based on the Swin Transformer, has provided a promising application in multi-source precipitation product fusion [13,160]. In parallel, unlike the standard supervised learning paradigm, which is typically trained directly on precipitation data from the target alpine region, transfer learning adopts a fundamentally different strategy [161]. It is initially pre-trained in data-rich regions to capture generalized spatiotemporal patterns, and the acquired knowledge is subsequently transferred and adapted to data-scarce high-altitude regions. Liu et al. [162] transferred a blending model pre-trained in eastern China to the TP, achieving a nearly 30% reduction in RMSE for the merged dataset relative to the original product.

However, in spite of the more advanced and complex architectures offered by DL models, their superior performance over traditional ML methods is not guaranteed [163]. Given that each category possesses distinct advantages, it is necessary to compare and select the most appropriate model for specific application contexts. Furthermore, integrating DL and traditional ML approaches within a hybrid framework leverages the advantages of both paradigms, potentially yielding greater overall benefits in precipitation product fusion. A representative example is a two-step "classification-regression" merging framework [7,164]. In this framework, precipitation events are first classified using traditional ML models, after which precipitation amount is quantified by more sophisticated DL networks. This design explicitly accounts for precipitation identification errors, which constitute a significant component of the total error in precipitation estimates [165].

5. Challenges and Future Recommendations

5.1. Product-Related Challenges and Recommendations

5.1.1. Inherent Error

SPPs and reanalysis datasets possess inherent limitations that constrain their accuracy in high-altitude regions, including limitations in orographic precipitation estimation and deficiencies in solid precipitation detection. Table 5 summarizes the major challenges and future research directions for precipitation products in high-altitude regions. Figure 10 provides a roadmap for future research in high-altitude precipitation estimation and application.

First, these datasets tend to exhibit a systematic bias, characterized by an overestimation of low precipitation rates and an underestimation of high-intensity events. This is partly attributed to the false detection of light rainfall and insufficient sensitivity to shallow orographic warm-rain processes. Reanalysis products further tend to overestimate total precipitation amounts. Second, estimating orographic precipitation remains a particularly formidable challenge due to the complex interactions between atmospheric flow and high-altitude terrain. It introduces additional uncertainties beyond those encountered in flat regions. Cloud microphysics are highly heterogeneous over mountainous terrain and are extremely unstable over short temporal and fine spatial scales [9], far exceeding the capturing capability of current satellite sensors. Furthermore, because of the limited spatial resolution of SPPs, one coarser pixel may simultaneously encompass multiple heterogeneous terrain types [166]. IR and PMW typically yield a mean precipitation estimate, rendering them unable to resolve sub-grid orographic precipitation gradients. Consequently, this limitation may lead to the underestimation of precipitation on windward slopes and overestimation on leeward slopes. To address these limitations, incorporating physically informed auxiliary information and utilizing reliable downscaling techniques are promising solutions. For example, He et al. [167] demonstrated that incorporating high-resolution thermodynamic and orographic information into a multi-channel infrared satellite precipitation retrieval framework can substantially improve heavy precipitation detection over complex terrain. Moreover, a topography-aware downscaling framework integrating terrain information with an AutoML-based scheme was used to refine coarse-resolution ERA5 precipitation to 90 m, effectively improving precipitation estimates and reducing wet biases over high-elevation and complex-terrain regions [168]. Third, significant challenges remain in the accurate quantification of solid precipitation in high-altitude and cold regions. On one hand, the decreased number of gauge samples constrains the bias correction of SPPs and reanalysis datasets in winter, as some gauges are unable to reliably monitor snowfall [169]. On the other hand, the influence of winds and other factors on gauges often leads to under-detection of snowfall events and underestimation of precipitation amounts [170,171]. Therefore, future developments should further improve solid precipitation retrieval and measurement techniques, and strengthen the integration of physically based information with satellite observations, particularly over snow- and ice-covered mountainous regions. Existing active-passive satellite observing frameworks, such as the combined use of the Dual-frequency Precipitation Radar (DPR) and GPM Microwave Imager (GMI) within the GPM mission, provide an important technical basis for improving precipitation-phase discrimination and snowfall retrieval [172].

Table 5. Summary of major challenges and future research directions.

Category	Identified Challenges	Underlying Causes	Recommended Future Research Directions
Product-related challenges	Inherent systematic biases and inadequate representation of orographic precipitation	Complex atmosphere-terrain interactions; heterogeneous cloud microphysics; limited sensor/grid resolution; unresolved sub-grid precipitation gradients	Incorporate physically informed auxiliary information and develop reliable downscaling methods for complex terrain
	Limited capability for solid precipitation quantification	Sparse winter gauges; unreliable snowfall measurements; wind-induced gauge undercatch	Improve solid precipitation retrieval and measurement techniques and explicitly account for snowfall measurement uncertainty
	Double-penalty error in precipitation evaluation	Small spatial or temporal displacement may be counted simultaneously as a miss and a false alarm in point-to-grid verification	Combine conventional point-based metrics with neighborhood-, scale-, and object-based verification approaches
	Spatial scale mismatch between gridded products and gauges	Gauges represent point precipitation, whereas gridded datasets represent area-averaged precipitation	Develop downscaling approaches that account for varying precipitation-topography relationships under different atmospheric conditions
Accuracy improvement algorithm challenges	Strong dependence of bias correction and merging on gauge observations	Correction and merging methods commonly rely on gauges for calibration, training, or weighting, making their performance sensitive to gauge availability and representativeness	Assess method performance under different gauge network densities, optimize methods for sparsely gauged regions, and quantify reference-data uncertainty and its propagation
	Restrictive assumptions in statistical correction and error-based merging	Conventional statistical correction commonly assumes stationarity; TC/ETC rely on assumptions concerning error independence, stationarity, additivity, or zero-mean errors	Develop methods that are more robust to non-stationary precipitation and correlated/non-additive product errors
	Limited interpretability, training data, and spatial coherence of ML approaches	Black-box characteristics; sparse and unrepresentative training observations; pixel-wise modeling neglects spatial dependence among neighboring grids	Develop physics-guided ML, zoning-based approaches accounting for climatic heterogeneity, and spatially explicit models that exploit neighboring-grid dependencies
Operational application challenges	Insufficient skill in simulating extreme precipitation and floods	Extreme-precipitation biases propagate into hydrological simulations; extreme-rainfall characteristics depend on duration and spatial scale	Evaluate extremes across multiple durations and hydrologically relevant scales, and integrate multi-sensor observations from active/passive remote sensing, reanalysis, and NWP information
	Insufficient spatiotemporal resolution	Coarse products fail to resolve the high heterogeneity of precipitation fields and the complex topography characteristic of small-scale catchments	Further develop high-resolution sensors and advanced downscaling techniques for small-basin and extreme-event applications
	Product latency and accuracy-timeliness trade-off	Final products may be delayed by weeks or months, whereas near-real-time versions have relatively larger errors	Complement observations with NWP and AI-based forecasts, accelerate processing using high-performance computing, and develop unified multi-source data-processing platforms

https://doi.org/10.3390/hydrology13090259

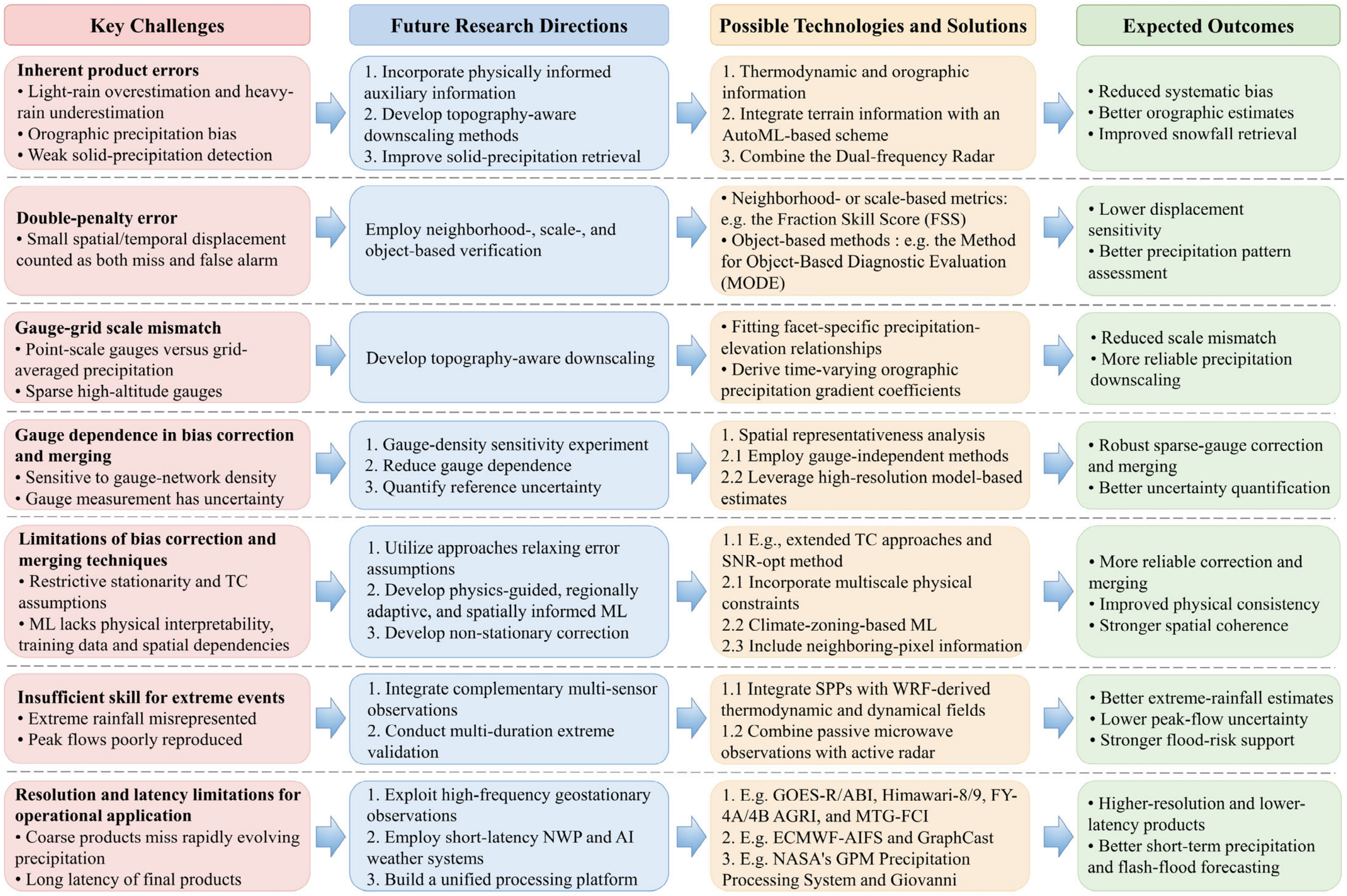

Figure 10. Roadmap for future research in high-altitude precipitation estimation and application.

5.1.2. Double-Penalty Error

Accuracy assessments of gridded precipitation datasets typically employ a "point-to-grid" comparison and utilize in-situ gauge observations as a reference. However, this approach might be susceptible to the double-penalty error when evaluating high spatiotemporal resolution products [173]. The double-penalty error arises when a precipitation event is correctly predicted but is slightly displaced in space or time relative to the gauge observation [174]. In such cases, the evaluation metric unfairly penalizes the product twice: once for a "miss" at the observed location, and again for a "false alarm" at the displaced location. This effect underestimates the actual skill of the dataset in capturing precipitation patterns, particularly in high-altitude regions where precipitation fields exhibit sharp spatial gradients and high temporal variability.

To address this issue, current research increasingly employs spatially tolerant verification approaches. Neighborhood- or scale-based metrics, such as the Fraction Skill Score (FSS) [175,176], assess precipitation agreement within spatial windows of increasing size rather than requiring exact grid-cell correspondence, thereby reducing penalties associated with small spatial displacements. In addition, object-based methods, such as the Method for Object-Based Diagnostic Evaluation (MODE) [177], identify contiguous precipitation features as spatial objects and evaluate their location, size, orientation, shape, and intensity separately. Therefore, future precipitation-product evaluations in high-altitude regions should combine conventional point-based metrics with neighborhood-, scale-, and object-based verification approaches to provide a more comprehensive assessment of spatial displacement and precipitation-pattern errors.

5.1.3. Mismatch of the Spatial Scale Between Gridded Precipitation Datasets and Gauge Measurements

Gauge observations reflect point-scale precipitation, whereas gridded precipitation products provide grid-averaged values. This spatial scale mismatch introduces skewed validation results and adds uncertainty to subsequent bias correction and data fusion procedures [13,178]. Downscaling offers a potential solution by refining gridded precipitation to a finer spatial resolution. However, downscaling daily precipitation remains highly challenging, as the spatial distribution of precipitation is influenced by multiple environmental variables, whose relationships with precipitation are highly unstable at the daily and sub-daily timescale [179]. For example, orographic precipitation-topography relationships have been shown to vary with both elevation and synoptic-scale atmospheric conditions, with cyclonically forced heavy precipitation events exhibiting markedly different precipitation-elevation gradients [180]. Therefore, it is advisable to develop downscaling models for varying precipitation-topography relationships under different atmospheric patterns. This concept has been preliminarily explored by Wolvin et al. [180]. They first partitioned mountainous terrain into topographically coherent facets, then fitted facet-specific linear or nonlinear precipitation-elevation relationships and derived temporally varying orographic precipitation-gradient coefficients, which were subsequently used to downscale coarse precipitation fields and better represent fine-scale orographic precipitation variability.

5.2. Accuracy Improvement Algorithm Challenges and Recommendations

5.2.1. Influence of Gauge Measurements on Bias Correction and Merging

The effectiveness of bias correction and merging with gauge observations is strongly dependent on the density of the rain gauge network. Correction and merging methods commonly rely on gauges for calibration, training, or weighting, making their performance sensitive to gauge availability and representativeness. This is particularly problematic on the southern slope of the TP, which exhibits distinct precipitation characteristics but merely has a sparse gauge network, leading to degraded accuracy of gridded precipitation products [77,169]. Therefore, further investigation into the applicability of various bias correction and fusion methods under different gauge network densities is needed, along with optimization of these methods for sparsely gauged regions.

It is also crucial to recognize that gauge observations should not be treated as error-free ground truth when evaluating or correcting SPPs. Gauge measurements themselves are subject to uncertainties arising from diverse climatic conditions, complex terrain, limited spatial representativeness, and instrumental errors [78,79]. These observational uncertainties are inevitably propagated into bias-corrected and merged precipitation products. In high-altitude regions, these limitations can be particularly severe, and recent studies suggest that well-configured high-resolution model-based precipitation estimates may, in some cases, better represent spatially integrated mountain precipitation than sparse gauge networks [181]. Current research increasingly investigates the sensitivity of correction and merging methods to gauge network density and spatial representativeness [182,183]. In parallel, gauge-independent approaches, such as improved TC methods, are being developed to reduce reliance on gauge measurements. Future research should place greater emphasis on quantifying reference-data uncertainty and tracing its propagation throughout the correction and fusion chain.

5.2.2. Limitations of Bias Correction and Merging Techniques

First, regarding conventional statistical methods of bias correction, they are predicated on the assumption of stationarity. However, precipitation trends and variability can experience substantial changes under evolving climatic conditions. Conventional statistical approaches risk weakening or artificially reshaping the true climate signal embedded in the original precipitation data. Future methods should further build on trend-preserving and non-stationary frameworks to improve their adaptability to changing climatic conditions.

Second, the TC method relies on the fundamental assumption that the errors among the three input products are mutually uncorrelated. In practice, however, this assumption is frequently violated, as some SPPs inevitably share common input sources or employ similar retrieval algorithms. Although the ETC method relaxes some constraints, its underlying assumption of stationary, additivity, and zero-mean errors may still be violated in complex terrain, where precipitation errors exhibit multiplicative behavior and non-zero conditional biases [184]. As an alternative approach, the SNR-opt does not require the assumption of zero error cross-correlation among products, offering greater flexibility in handling correlated errors. However, it requires prior knowledge or reliable estimation of the signal-to-noise ratio for each product, which is often difficult to obtain, particularly in data-sparse regions [27].

Third, ML techniques face inherent limitations regarding physical interpretability, data scarcity, and spatial coherence. They operate as "black boxes", establishing complex non-linear mappings between inputs and outputs without revealing the underlying mechanisms. While they can yield favorable statistical metrics, the lack of interpretability makes it difficult to identify extrapolation risks for extreme events or spatial generalization capabilities in ungauged high-altitude regions. To mitigate this, incorporating physical mechanisms to construct physics-guided bias correction or merging approaches can enhance the physical consistency of generated precipitation products. One pathway that has been demonstrated to be effective in enhancing the physical feasibility is the incorporation of multiscale physical constraints, including local pixel-wise physical conditions and global rainfall conservation, into data-driven precipitation correction frameworks [185].

Furthermore, the accuracy of ML models heavily depends on the quantity and representativeness of observation samples. Sparse gauge networks in high-altitude regions prevent models from establishing robust statistical relationships, limiting their ability to effectively learn the error characteristics of precipitation products. Recent work has sought to overcome this challenge by adopting zoning-based approaches, which couple spatially coherent sub-regions with ML, while accounting for regional climate heterogeneity [186]. This integrated method improves product performance and strengthens the generalizability of correction models across spatial domains.

Conventional ML approaches typically establish relationships between gridded features and gauge observations independently at each pixel, neglecting the spatial dependencies of neighboring grids. However, precipitation fields exhibit strong spatial correlation, with each grid point influencing its surroundings [187]. This is particularly problematic in high-altitude regions where topography-precipitation interactions are complex. Future research should therefore place greater emphasis on fully exploiting these spatial features in ML modeling, which holds significant potential for improving the accuracy of precipitation products [188]. For instance, spatially informed random forest frameworks, which explicitly integrate spatial autocorrelation among neighboring precipitation pixels, provide a preliminary pathway to merge precipitation products by leveraging surrounding spatial information [189].

5.3. Operational Application Challenges and Recommendations

5.3.1. Insufficient Skill in Simulating Extreme Events

As demonstrated in the preceding sections, both SPPs and reanalysis datasets tend to overestimate the occurrence of torrential and extreme precipitation events in high-altitude basins. When SPPs are used as inputs to hydrological models, this bias can propagate into flood simulations, leading to deviations in peak flow predictions. Similarly, reanalysis datasets often show limited capability in reproducing extreme runoff characteristics and may underestimate peak flows. Consequently, these gridded precipitation products introduce considerable uncertainty into the representation of extreme events. This issue is further complicated by the fact that extreme-rainfall trends are strongly dependent on event duration and spatial scale. Increasing trends may be pronounced at short durations but weaken or disappear at longer durations, while substantial spatial heterogeneity can occur even within the same region [190]. Therefore, satisfactory performance at the daily scale does not necessarily imply that a gridded product can reliably reproduce sub-daily extremes, local trend hotspots, or their non-stationary behavior. Extreme-precipitation validation should be conducted across multiple durations and at hydrologically relevant spatial scales.

Further efforts are still needed to improve the simulation of extremes in high-altitude regions, including both extreme precipitation and extreme floods. Because extreme weather events involve complex interactions among multiple atmospheric and land surface processes [191], relying on a single satellite observation source is unlikely to capture these interactions adequately. Future research could therefore further integrate multi-sensor observations, including active and passive remote sensing, and numerical weather prediction (NWP) models. A step in this direction has been taken by an emerging ML-based framework that integrates SPPs with high-resolution WRF-derived thermodynamic and dynamical fields, providing a preliminary pathway for improving intense rainfall estimation and holding particular promise for application in high-altitude basins [192]. Active-passive sensor integration has also demonstrated considerable potential for reconstructing three-dimensional precipitation structures during extreme rainfall events. For instance, a recent FY-3G framework used DL to combine passive MWRI-RM multi-channel microwave observations with active PMR-Ku radar measurements, enabling improved representation of high-reflectivity structures during typhoon and extreme-rainfall events [193].

5.3.2. Spatiotemporal Resolution and Latency Limitations

Despite substantial advancements in satellite observation technology, achieving high spatiotemporal resolution for specific applications, such as hourly flood forecasting and hydrological simulation in small basins, remains a critical challenge. These applications require frequent and detailed observations to capture the rapid evolution of hydrological processes, which often occur within short time windows and over localized areas [105]. Coarse-resolution products often fail to resolve the high heterogeneity of precipitation fields and the complex topography characteristic of small-scale catchments. Continuous development of high-resolution sensors and advanced downscaling techniques is essential for more accurate representation of precipitation fields at the scales required for extreme event simulation and forecasting. The increasing availability of high-temporal-resolution GEO satellite observations, such as GOES-R/ABI, Himawari-8/9 AHI, FY-4A/4B AGRI, and MTG-FCI, provides new opportunities to resolve rapidly evolving convective precipitation at minute-scale intervals and thereby improve short-term precipitation and flash-flood forecasting.

Additionally, the latency of SPP and reanalysis datasets poses another significant limitation for operational applications. On one hand, for precipitation nowcasting and near-real-time flood forecasting, gridded precipitation products with short latency are essential. However, the final release versions of SPP and reanalysis datasets typically become available weeks or even months after the observation date, and their pre-released near-real-time counterparts often suffer from relatively larger errors. To address this gap, short-latency NWP forecasts and emerging AI-based weather prediction systems, such as ECMWF-

AIFS [194] and GraphCast [195], may provide complementary precipitation information. On the other hand, improving the efficiency of satellite data retrieval, extraction, and interpretation is of great importance as well. It is advisable to develop high-performance computing algorithms to expedite remote sensing data processing and reduce output latency, thereby meeting the real-time requirements of operational hydrological applications. Furthermore, constructing a unified processing platform that integrates capabilities such as data retrieval, quality assurance, format standardization, and interface provision for multi-source observation data can also enhance the efficiency of data processing [196]. In this context, NASA's GPM Precipitation Processing System and Giovanni serve as excellent exemplars for implementing such a platform.

6. Conclusions

The paper provides a comprehensive review of the application of SPPs and reanalysis datasets in high-altitude regions characterized by sparse gauge networks and complex terrain. First, the theoretical basis, comparative advantages, and representative products of SPPs and reanalysis datasets are introduced. Constrained by intricate climatic conditions, complex topography, and sparse gauge observations inherent to high-altitude regions, SPPs and reanalysis datasets offer distinct advantages in terms of spatiotemporal continuity and quasi-global coverage for these remote and inaccessible regions. Although they serve as effective alternatives for quantitative precipitation estimation and hydrological simulation, these products still suffer from errors arising from observation, sampling, and retrieval algorithms. Following the review of data sources, a critical applicability assessment of these gridded precipitation products in high-altitude regions, with particular emphasis on the TP, is presented. Owing to their inherent errors, both SPPs and reanalysis datasets show non-negligible systematic biases over the TP. They consistently tend to overestimate low precipitation rates while underestimating high precipitation rates. In addition, they exhibit pronounced conditional biases across spatial, seasonal, and daily scales. Regarding hydrological performance, these products are insufficient to capture extreme runoff features and tend to underestimate peak flows. Accordingly, these notable errors necessitate accuracy improvement prior to the application of gridded precipitation datasets in high-altitude regions. The paper subsequently reviews the theoretical foundations of single-product bias correction and product merging techniques, along with their implementation procedures and case studies in high-altitude regions. These two methods have been shown to significantly reduce errors in precipitation estimates and hydrological simulations. Nevertheless, remaining challenges related to the products themselves, accuracy improvement algorithms, and operational applications are identified. Meanwhile, corresponding recommendations for future research are presented:

(1) SPPs and reanalysis products inevitably have inherent errors from limitations in orographic precipitation estimation and deficiencies in solid precipitation detection. Furthermore, the double-penalty error and scale mismatch between gridded precipitation datasets and point-scale gauge measurements warrant particular attention when evaluating and correcting these products in complex terrain. Both factors can introduce biased validation outcomes and inject additional uncertainty into subsequent bias correction and data fusion procedures. Promising avenues for addressing these issues include enhancing physical constraints into precipitation retrieval algorithms and developing downscaling techniques that account for varying precipitation-topography relationships.

(2) Regarding accuracy improvement algorithm challenges, the effectiveness of bias correction and product merging methods that incorporate gauge observations heavily depends on the density of rain gauge networks. This issue is clearly exemplified

over the TP. Bias-corrected or fused precipitation products exhibit notably poorer accuracy on the gauge-scarce southern slope compared to those in the gauge-denser eastern part of the plateau. Moreover, uncertainties from gauge observations can propagate through the correction or fusion algorithm into reconstructed precipitation products. Therefore, future research can prioritize the optimization of accuracy improvement algorithms for regions with varying gauge network densities, as well as the quantification of uncertainty propagation from gauge measurements. In addition, different accuracy improvement algorithms possess distinct advantages and limitations. The selection of an appropriate algorithm should be guided by the specific application context.

(3) SPPs and reanalysis datasets remain insufficient for simulating extreme events in high-altitude areas, whether through direct quantitative precipitation estimation or through their use as inputs to hydrologic models. Further efforts are still needed to improve the simulation accuracy of extreme precipitation and extreme floods. Recommended strategies include integrating multi-sensor observations, adopting high-resolution datasets, employing short-lag or AI-based forecast products, and developing a unified data-processing platform to support operational applications.

This review provides guidance for leveraging gridded precipitation products to enhance precipitation monitoring, mitigate extreme precipitation and flood disasters, and deepen understanding of climate variability.

Author Contributions: Conceptualization, L.D. and S.S.; writing-original draft preparation, L.D.; writing-review and editing, S.S., H.C., X.Z., Y.Z. and G.Z.; visualization, L.D. and F.W.; supervision, S.S., H.C. and X.Z.; funding acquisition, H.C. All authors have read and agreed to the published version of the manuscript.

Funding: This research was funded by the National Key Research and Development Program of China (Grant No.2023YFC3209101) and PowerChina (Grant No.DJ-HXGG-2025-02).

Data Availability Statement: No new data were created or analyzed in this study. Data sharing is not applicable to this article.

Acknowledgments: We appreciate the editors and anonymous reviewers for enhancing our paper. During the preparation of this manuscript, the authors used ChatGPT (OpenAI, GPT-5 series) for language refinement. The authors have reviewed and edited the output and take full responsibility for the content of this publication.

Conflicts of Interest: The authors declare no conflicts of interest. Authors Liangkun Deng, Shihan Shan, Guiliang Zhong, Fuling Wen, and Yan Zhang were employed by the company PowerChina Chengdu Engineering Corporation Limited. The remaining authors declare that the research was conducted in the absence of any commercial or financial relationships that could be construed as a potential conflict of interest.

References

1. Kidd, C.; Huffman, G. Global Precipitation Measurement. *Meteorol. Appl.* **2011**, *18*, 334–353. [CrossRef]
2. Trenberth, K.E.; Dai, A.; Rasmussen, R.M.; Parsons, D.B. The Changing Character of Precipitation. *Bull. Am. Meteorol. Soc.* **2003**, *84*, 1205–1218. [CrossRef]
3. Nourani, V.; Tosan, M.; Huang, J.J.; Gebremichael, M.; Kantoush, S.A.; Dastourani, M. Advances in Multi-Source Data Fusion for Precipitation Estimation: Remote Sensing and Machine Learning Perspectives. *Earth-Sci. Rev.* **2025**, *270*, 105253. [CrossRef]
4. Curio, J.; Scherer, D. Seasonality and Spatial Variability of Dynamic Precipitation Controls On the Tibetan Plateau. *Earth Syst. Dyn.* **2016**, *7*, 767–782. [CrossRef]
5. Michaelides, S.; Levizzani, V.; Anagnostou, E.; Bauer, P.; Kasparis, T.; Lane, J.E. Precipitation: Measurement, Remote Sensing, Climatology and Modeling. *Atmos. Res.* **2009**, *94*, 512–533. [CrossRef]

6. Kidd, C.; Becker, A.; Huffman, G.J.; Muller, C.L.; Joe, P.; Skofronick-Jackson, G.; Kirschbaum, D.B. So, How Much of the Earth'S Surface is Covered by Rain Gauges? *Bull. Am. Meteorol. Soc.* **2017**, *98*, 69–78. [CrossRef]
7. Lyu, Y.; Yong, B. A Novel Double Machine Learning Strategy for Producing High-Precision Multi-Source Merging Precipitation Estimates Over the Tibetan Plateau. *Water Resour. Res.* **2024**, *60*, e2023WR035643. [CrossRef]
8. Chang, C.; Chen, Y.; Huang, J.J. Variability of Rainfall Areal Reduction Factors for a Coastal City: A Case Study of Shenzhen, China. *J. Hydrol. Eng.* **2023**, *28*, 5023008. [CrossRef]
9. Gou, Y.; Ma, Y.; Chen, H.; Wen, Y. Radar-Derived Quantitative Precipitation Estimation in Complex Terrain Over the Eastern Tibetan Plateau. *Atmos. Res.* **2018**, *203*, 286–297. [CrossRef]
10. Sun, Q.; Miao, C.; Duan, Q.; Ashouri, H.; Sorooshian, S.; Hsu, K.L. A Review of Global Precipitation Data Sets: Data Sources, Estimation, and Intercomparisons. *Rev. Geophys.* **2018**, *56*, 79–107. [CrossRef]
11. Jahanshahi, A.; Roshun, S.H.; Booij, M.J. Comparison of Satellite-Based and Reanalysis Precipitation Products for Hydrological Modeling Over a Data-Scarce Region. *Clim. Dyn.* **2024**, *62*, 3505–3537. [CrossRef]
12. Mankin, K.R.; Mehan, S.; Green, T.R.; Barnard, D.M. Review of Gridded Climate Products and their Use in Hydrological Analyses Reveals Overlaps, Gaps, and the Need for a More Objective Approach to Selecting Model Forcing Datasets. *Hydrol. Earth Syst. Sci.* **2025**, *29*, 85–108. [CrossRef]
13. Zhang, Y.; Wang, Q.J.; Frost, A.J.; Trewin, B.; Pudashine, J.; Velasco Forero, C.; Su, C.H.; Villani, V. Advancing High-Resolution Precipitation Analysis for Operational Hydrological Applications in Australia: Data Sources, Methodologies, and Recommendations. *Wiley Interdiscip. Rev. Water* **2025**, *12*, e70037. [CrossRef]
14. Wei, L.; Jiang, S.; Ren, L.; Hua, Z.; Zhang, L.; Zeng, L.; Duan, Z. An Algorithm to Improve Satellite-Only Precipitation Estimates Over the Tibetan Plateau. *Atmos. Res.* **2026**, *339*, 109035. [CrossRef]
15. Tan, A.; Li, M.; Liu, H.; Chen, L.; Wang, T.; Wang, W.; Shi, Y. Comparative Assessment of Eight Satellite Precipitation Products Over the Complex Terrain of the Lower Yarlung Zangpo Basin: Performance Evaluation and Topographic Influence Analysis. *Remote Sens.* **2026**, *18*, 63. [CrossRef]
16. Liu, Z. Comprehensive Evaluation of High-Resolution Satellite Precipitation Products Over the Qinghai–Tibetan Plateau Using the New Ground Observation Network. *Remote Sens.* **2023**, *15*, 3381. [CrossRef]
17. Fan, M.; Xu, J.; Li, D.; Chen, Y. Response of Precipitation in Tianshan to Global Climate Change Based On the Berkeley Earth and ERA5 Reanalysis Products. *Remote Sens.* **2022**, *14*, 519. [CrossRef]
18. Chen, Y.; Sharma, S.; Zhou, X.; Yang, K.; Li, X.; Niu, X.; Hu, X.; Khadka, N. Spatial Performance of Multiple Reanalysis Precipitation Datasets On the Southern Slope of Central Himalaya. *Atmos. Res.* **2021**, *250*, 105365. [CrossRef]
19. Anand, A.; Garg, V.K. Temperature–Precipitation Trends and Response of High-Altitude Biodiversity Reserve of Western Himalayas. *J. Earth Syst. Sci.* **2024**, *133*, 76. [CrossRef]
20. Beck, H.E.; Vergopolan, N.; Pan, M.; Levizzani, V.; Van Dijk, A.I.; Weedon, G.P.; Brocca, L.; Pappenberger, F.; Huffman, G.J.; Wood, E.F. Global-Scale Evaluation of 22 Precipitation Datasets Using Gauge Observations and Hydrological Modeling. *Hydrol. Earth Syst. Sci.* **2017**, *21*, 6201–6217. [CrossRef]
21. Guragain, S.; Shah, S.; Albano, R.; Kim, S.; Hammad, M.; Asif, M. Quantifying the Added Values of a Merged Precipitation Product in Streamflow Prediction Over the Central Himalayas. *Remote Sens.* **2025**, *17*, 2170. [CrossRef]
22. Maggioni, V.; Massari, C. On the Performance of Satellite Precipitation Products in Riverine Flood Modeling: A Review. *J. Hydrol.* **2018**, *558*, 214–224. [CrossRef]
23. Hinge, G.; Hamouda, M.A.; Long, D.; Mohamed, M.M. Hydrologic Utility of Satellite Precipitation Products in Flood Prediction: A Meta-Data Analysis and Lessons Learnt. *J. Hydrol.* **2022**, *612*, 128103. [CrossRef]
24. Zhang, M.; Li, J.; Li, N.; Sun, W.; Li, P.; Zhao, Y. Spatial Inhomogeneity of Synoptic-Induced Precipitation in a Region of Steep Topographic Relief: A Case Study. *J. Geophys. Res. Atmos.* **2024**, *129*, e2023JD039129. [CrossRef]
25. Bookhagen, B.; Burbank, D.W. Topography, Relief, and TRMM-Derived Rainfall Variations Along the Himalaya. *Geophys. Res. Lett.* **2006**, *33*, 2006GL026037. [CrossRef]
26. Kim, S.; Sharma, A.; Liu, Y.Y.; Young, S.I. Rethinking Satellite Data Merging: From Averaging to SNR Optimization. *IEEE Trans. Geosci. Remote Sens.* **2022**, *60*, 1–15. [CrossRef]
27. Shah, S.; Liu, Y.; Kim, S.; Sharma, A. Advancing High-Mountain Precipitation Reconstruction through Merging of Multiple Data Sources: Triple Collocation Versus Signal-to-Noise Ratio Optimization. *IEEE Trans. Geosci. Remote Sens.* **2024**, *62*, 4212315. [CrossRef]
28. Yin, J.; Guo, S.; Gu, L.; Zeng, Z.; Liu, D.; Chen, J.; Shen, Y.; Xu, C. Blending Multi-Satellite, Atmospheric Reanalysis and Gauge Precipitation Products to Facilitate Hydrological Modelling. *J. Hydrol.* **2021**, *593*, 125878. [CrossRef]
29. Chen, H.; Sun, L.; Cifelli, R.; Xie, P. Deep Learning for Bias Correction of Satellite Retrievals of Orographic Precipitation. *IEEE Trans. Geosci. Remote Sens.* **2022**, *60*, 4104611. [CrossRef]
30. Nan, T.; Chen, J.; Ding, Z.; Li, W.; Chen, H. Deep Learning-Based Multi-Source Precipitation Merging for the Tibetan Plateau. *Sci. China Earth Sci.* **2023**, *66*, 852–870. [CrossRef]

31. Sambyal, S.; Shastri, S.; Taloor, A.K.; Kumar, A.; Mansotra, V. Statistical and Machine Learning-Based Bias-Correction of ERA5 Forcing Data: Implications for Himalayan Glacier Melt Modelling. *Phys. Chem. Earth Parts A/B/C* **2026**, *143*, 104387. [CrossRef]
32. Saha, A.; Chandra Pal, S. Application of Machine Learning and Emerging Remote Sensing Techniques in Hydrology: A State-of-the-Art Review and Current Research Trends. *J. Hydrol.* **2024**, *632*, 130907. [CrossRef]
33. Belay, H.; Melesse, A.M.; Tegegne, G. Merging Satellite Products and Rain-Gauge Observations to Improve Hydrological Simulation: A Review. *Earth* **2022**, *3*, 1275–1289. [CrossRef]
34. Lyu, Y.; Yong, B.; Huang, F.; Qi, W.; Tian, F.; Wang, G.; Zhang, J. Investigating Twelve Mainstream Global Precipitation Datasets: Which One Performs Better On the Tibetan Plateau? *J. Hydrol.* **2024**, *633*, 130947. [CrossRef]
35. Cheng, Y.; Zhang, X.; Wang, K.; Zhang, Y.; Guo, Y.; Shen, Y. Multidimensional Evaluation of Satellite-Based and Reanalysis-Based Precipitation Datasets in the Tibetan Plateau. *J. Hydrol.* **2025**, *660*, 133364. [CrossRef]
36. Hirpa, F.A.; Gebremichael, M.; Hopson, T. Evaluation of High-Resolution Satellite Precipitation Products Over Very Complex Terrain in Ethiopia. *J. Appl. Meteorol. Climatol.* **2010**, *49*, 1044–1051. [CrossRef]
37. Derin, Y.; Anagnostou, E.; Berne, A.; Borga, M.; Boudevillain, B.; Buytaert, W.; Chang, C.; Delrieu, G.; Hong, Y.; Hsu, Y.C.; et al. Multiregional Satellite Precipitation Products Evaluation Over Complex Terrain. *J. Hydrometeorol.* **2016**, *17*, 1817–1836. [CrossRef]
38. Huffman, G.J.; Bolvin, D.T.; Nelkin, E.J.; Wolff, D.B.; Adler, R.F.; Gu, G.; Hong, Y.; Bowman, K.P.; Stocker, E.F. The TRMM Multisatellite Precipitation Analysis (TMPA): Quasi-Global, Multiyear, Combined-Sensor Precipitation Estimates at Fine Scales. *J. Hydrometeorol.* **2007**, *8*, 38–55. [CrossRef]
39. Huffman, G.J.; Bolvin, D.T.; Braithwaite, D.; Hsu, K.; Joyce, R.; Xie, P.; Yoo, S. NASA Global Precipitation Measurement (GPM) Integrated Multi-Satellite Retrievals for GPM (IMERG). *Algorithm Theor. Basis Doc.* **2015**, *4*, 30.
40. Mega, T.; Ushio, T.; Takahiro, M.; Kubota, T.; Kachi, M.; Oki, R. Gauge-Adjusted Global Satellite Mapping of Precipitation. *IEEE Trans. Geosci. Remote Sens.* **2019**, *57*, 1928–1935. [CrossRef]
41. Joyce, R.J.; Janowiak, J.E.; Arkin, P.A.; Xie, P. CMORPH: A Method that Produces Global Precipitation Estimates From Passive Microwave and Infrared Data at High Spatial and Temporal Resolution. *J. Hydrometeorol.* **2004**, *5*, 487–503. [CrossRef]
42. Funk, C.; Peterson, P.; Harrison, L.; Saldivar, R.; Landsfeld, M.; Pedreros, D.; Shukla, S.; Fink, A.H.; Davenport, F.; Peterson, S. The Climate Hazards Center Infrared Precipitation with Stations, Version 3. *Sci. Data* **2026**, *13*, 718. [CrossRef]
43. Bolboli Zadeh, M.; Nguyen, P.; Hsu, K.; AghaKouchak, A.; Thanh Ung, T.; Sorooshian, S. A Global High-Resolution Precipitation Climate Record: PERSIANN-CCS-CDR Version 2.0. *Sci. Data* **2026**, *13*, 314. [CrossRef]
44. Nguyen, P.; Ombadi, M.; Gorooh, V.A.; Shearer, E.J.; Sadeghi, M.; Sorooshian, S.; Hsu, K.; Bolvin, D.; Ralph, M.F. PERSIANN Dynamic Infrared–Rain Rate (PDIR-Now): A Near-Real-Time, Quasi-Global Satellite Precipitation Dataset. *J. Hydrometeorol.* **2020**, *21*, 2893–2906. [CrossRef]
45. Nguyen, P.; Shearer, E.J.; Tran, H.; Ombadi, M.; Hayatbini, N.; Palacios, T.; Huynh, P.; Braithwaite, D.; Updegraff, G.; Hsu, K.; et al. The CHRS Data Portal, an Easily Accessible Public Repository for PERSIANN Global Satellite Precipitation Data. *Sci. Data* **2019**, *6*, 180296. [CrossRef]
46. Lu, X.; Tang, G.; Wang, X.; Liu, Y.; Jia, L.; Xie, G.; Li, S.; Zhang, Y. Correcting GPM IMERG Precipitation Data Over the Tianshan Mountains in China. *J. Hydrol.* **2019**, *575*, 1239–1252. [CrossRef]
47. Sharma, S.; Khadka, N.; Hamal, K.; Shrestha, D.; Talchabhadel, R.; Chen, Y. How Accurately Can Satellite Products (TMPA and IMERG) Detect Precipitation Patterns, Extremities, and Drought Across the Nepalese Himalaya? *Earth Space Sci.* **2020**, *7*, e2020EA001315. [CrossRef]
48. Ba, M.B.; Gruber, A. GOES Multispectral Rainfall Algorithm (GMSRA). *J. Appl. Meteorol.* **2001**, *40*, 1500–1514. [CrossRef]
49. Funk, C.; Peterson, P.; Landsfeld, M.; Pedreros, D.; Verdin, J.; Shukla, S.; Husak, G.; Rowland, J.; Harrison, L.; Hoell, A.; et al. The Climate Hazards Infrared Precipitation with Stations—A New Environmental Record for Monitoring Extremes. *Sci. Data* **2015**, *2*, 150066. [CrossRef]
50. Hsu, K.; Gao, X.; Sorooshian, S.; Gupta, H.V. Precipitation Estimation From Remotely Sensed Information Using Artificial Neural Networks. *J. Appl. Meteorol.* **1997**, *36*, 1176–1190. [CrossRef]
51. Kummerow, C.; Hong, Y.; Olson, W.S.; Yang, S.; Adler, R.F.; McCollum, J.; Ferraro, R.; Petty, G.; Shin, D.; Wilheit, T.T. The Evolution of the Goddard Profiling Algorithm (GPROF) for Rainfall Estimation From Passive Microwave Sensors. *J. Appl. Meteorol.* **2001**, *40*, 1801–1820. [CrossRef]
52. Elsaesser, G.S.; Kummerow, C.D. The Sensitivity of Rainfall Estimation to Error Assumptions in a Bayesian Passive Microwave Retrieval Algorithm. *J. Appl. Meteorol. Climatol.* **2015**, *54*, 408–422. [CrossRef]
53. Prigent, C.; Jimenez, C.; Aires, F. Toward "All Weather," Long Record, and Real-Time Land Surface Temperature Retrievals From Microwave Satellite Observations. *J. Geophys. Res. Atmos.* **2016**, *121*, 5699–5717. [CrossRef]
54. Afzali Gorooh, V.; Petković, V.; Arulraj, M.; Nguyen, P.; Hsu, K.; Sorooshian, S.; Ferraro, R.R. Integrating LEO and GEO Observations: Toward Optimal Summertime Satellite Precipitation Retrieval. *J. Hydrometeorol.* **2023**, *24*, 1939–1954. [CrossRef]
55. Kidd, C.; Levizzani, V. Status of Satellite Precipitation Retrievals. *Hydrol. Earth Syst. Sci.* **2011**, *15*, 1109–1116. [CrossRef]

56. Zhang, P.; Gu, S.; Chen, L.; Shang, J.; Lin, M.; Zhu, A.; Yin, H.; Wu, Q.; Shou, Y.; Sun, F.; et al. FY-3G Satellite Instruments and Precipitation Products: First Report of China'S Fengyun Rainfall Mission in-Orbit. *J. Remote Sens.* **2023**, *3*, 97. [CrossRef]
57. Kummerow, C.D.; Simpson, J.; Thiele, O.W.; Barnes, W.; Chang, A.T.C.; Stocker, E.F.; Adler, R.F.; Hou, A.Y.; Kakar, R.K.; Wentz, F.; et al. The Status of the Tropical Rainfall Measuring Mission (TRMM) After Two Years in Orbit. *J. Appl. Meteorol.* **2000**, *39*, 1965–1982. [CrossRef]
58. Kubota, T.; Shige, S.; Hashizume, H.; Aonashi, K.; Takahashi, N.; Seto, S.; Hirose, M.; Takayabu, Y.N.; Ushio, T.; Nakagawa, K.; et al. Global Precipitation Map Using Satellite-Borne Microwave Radiometers by the GSMaP Project: Production and Validation. *IEEE Trans. Geosci. Remote Sens.* **2007**, *45*, 2259–2275. [CrossRef]
59. Jones, R.W.; Renfrew, I.A.; Orr, A.; Webber, B.G.M.; Holland, D.M.; Lazzara, M.A. Evaluation of Four Global Reanalysis Products Using in Situ Observations in the Amundsen Sea Embayment, Antarctica. *J. Geophys. Res. Atmos.* **2016**, *121*, 6240–6257. [CrossRef]
60. Yin, J.; Liang, X.; Xie, Y.; Li, F.; Hu, K.; Cao, L.; Chen, F.; Zou, H.; Zhu, F.; Sun, X.; et al. East Asia Reanalysis System (EARS). *Earth Syst. Sci. Data Discuss.* **2023**, *2023*, 1–44. [CrossRef]
61. Hersbach, H.; Bell, B.; Berrisford, P.; Hirahara, S.; Horányi, A.; Muñoz Sabater, J.; Nicolas, J.; Peubey, C.; Radu, R.; Schepers, D.; et al. The ERA5 Global Reanalysis. *Q. J. R. Meteorol. Soc.* **2020**, *146*, 1999–2049. [CrossRef]
62. Muñoz-Sabater, J.; Dutra, E.; Agustí-Panareda, A.; Albergel, C.; Arduini, G.; Balsamo, G.; Boussetta, S.; Choulga, M.; Harrigan, S.; Hersbach, H. ERA5-Land: A State-of-the-Art Global Reanalysis Dataset for Land Applications. *Earth Syst. Sci. Data Discuss.* **2021**, *2021*, 1–50. [CrossRef]
63. Rodell, M.; Houser, P.R.; Jambor, U.; Gottschalck, J.; Mitchell, K.; Meng, C.J.; Arsenault, K.R.; Cosgrove, B.; Radakovich, J.; Bosilovich, M.G.; et al. The Global Land Data Assimilation System. *Bull. Am. Meteorol. Soc.* **2004**, *85*, 381–394. [CrossRef]
64. Gelaro, R.; McCarty, W.; Suárez, M.J.; Todling, R.; Molod, A.; Takacs, L.; Randles, C.A.; Darmenov, A.; Bosilovich, M.G.; Reichle, R.; et al. The Modern-Era Retrospective Analysis for Research and Applications, Version 2 (MERRA-2). *J. Clim.* **2017**, *30*, 5419–5454. [CrossRef]
65. Kobayashi, S.; Ota, Y.; Harada, Y.; Ebita, A.; Moriya, M.; Onoda, H.; Onogi, K.; Kamahori, H.; Kobayashi, C.; Endo, H. The JRA-55 Reanalysis: General Specifications and Basic Characteristics. *J. Meteorol. Soc. Jpn. Ser. II* **2015**, *93*, 5–48. [CrossRef]
66. Kosaka, Y.; Kobayashi, S.; Harada, Y.; Kobayashi, C.; Naoe, H.; Yoshimoto, K.; Harada, M.; Goto, N.; Chiba, J.; Miyaoka, K.; et al. The JRA-3Q Reanalysis. *J. Meteorol. Soc. Jpn. Ser. II* **2024**, *102*, 49–109. [CrossRef]
67. Kanamitsu, M.; Ebisuzaki, W.; Woollen, J.; Yang, S.; Hnilo, J.J.; Fiorino, M.; Potter, G.L. NCEP-DOE AMIP-II Reanalysis (R-2). *Bull. Am. Meteorol. Soc.* **2002**, *83*, 1631–1644. [CrossRef]
68. Xia, Y.; Mitchell, K.; Ek, M.; Sheffield, J.; Cosgrove, B.; Wood, E.; Luo, L.; Alonge, C.; Wei, H.; Meng, J.; et al. Continental-Scale Water and Energy Flux Analysis and Validation for the North American Land Data Assimilation System Project Phase 2 (NLDAS-2): 1. Intercomparison and Application of Model Products. *J. Geophys. Res. Atmos.* **2012**, *117*, 2011JD016048.
69. Shi, C.; Jiang, L.; Zhang, T.; Xu, B.; Han, S. Status and Plans of CMA Land Data Assimilation System (CLDAS) Project. *EGU Gen. Assem. Conf. Abstr.* **2014**, *16*, EGU2014-5671.
70. Lavers, D.A.; Simmons, A.; Vamborg, F.; Rodwell, M.J. An Evaluation of ERA5 Precipitation for Climate Monitoring. *Q. J. R. Meteorol. Soc.* **2022**, *148*, 3152–3165. [CrossRef]
71. Ji, L.; Senay, G.B.; Verdin, J.P. Evaluation of the Global Land Data Assimilation System (GLDAS) Air Temperature Data Products. *J. Hydrometeorol.* **2015**, *16*, 2463–2480. [CrossRef]
72. Xia, Y.; Ek, M.; Wei, H.; Meng, J. Comparative Analysis of Relationships Between NLDAS-2 Forcings and Model Outputs. *Hydrol. Process.* **2012**, *26*, 467–474. [CrossRef]
73. Xia, Y.; Mitchell, K.; Ek, M.; Cosgrove, B.; Sheffield, J.; Luo, L.; Alonge, C.; Wei, H.; Meng, J.; Livneh, B.; et al. Continental-Scale Water and Energy Flux Analysis and Validation for North American Land Data Assimilation System Project Phase 2 (NLDAS-2): 2. Validation of Model-Simulated Streamflow. *J. Geophys. Res. Atmos.* **2012**, *117*, 2011JD016051.
74. Han, S.; Liu, B.; Shi, C.; Liu, Y.; Qiu, M.; Sun, S. Evaluation of CLDAS and GLDAS Datasets for Near-Surface Air Temperature Over Major Land Areas of China. *Sustainability* **2020**, *12*, 4311.
75. Derin, Y.; Anagnostou, E.; Berne, A.; Borga, M.; Boudevillain, B.; Buytaert, W.; Chang, C.; Chen, H.; Delrieu, G.; Hsu, Y.C. Evaluation of GPM-Era Global Satellite Precipitation Products Over Multiple Complex Terrain Regions. *Remote Sens.* **2019**, *11*, 2936. [CrossRef]
76. Satgé, F.; Ruelland, D.; Bonnet, M.; Molina, J.; Pillco, R. Consistency of Satellite-Based Precipitation Products in Space and Over Time Compared with Gauge Observations and Snow-Hydrological Modelling in the Lake Titicaca Region. *Hydrol. Earth Syst. Sci.* **2019**, *23*, 595–619. [CrossRef]
77. Zhang, W.; Di, Z.; Liu, J.; Zhang, S.; Liu, Z.; Wang, X.; Sun, H. Evaluation of Five Satellite-Based Precipitation Products for Extreme Rainfall Estimations Over the Qinghai-Tibet Plateau. *Remote Sens.* **2023**, *15*, 5379. [CrossRef]
78. Lei, H.; Zhao, H.; Ao, T. A Two-Step Merging Strategy for Incorporating Multi-Source Precipitation Products and Gauge Observations Using Machine Learning Classification and Regression Over China. *Hydrol. Earth Syst. Sci. Discuss.* **2022**, *2022*, 1–33. [CrossRef]

79. Ma, Y.; Zhang, Y.; Yang, D.; Farhan, S.B. Precipitation Bias Variability Versus Various Gauges Under Different Climatic Conditions Over the Third Pole Environment (TPE) Region. *Int. J. Climatol.* **2015**, *35*, 1201–1211. [CrossRef]
80. Bosilovich, M.G.; Chen, J.; Robertson, F.R.; Adler, R.F. Evaluation of Global Precipitation in Reanalyses. *J. Appl. Meteorol. Climatol.* **2008**, *47*, 2279–2299. [CrossRef]
81. Dunn, R.J.H.; Donat, M.G.; Alexander, L.V. Comparing Extremes Indices in Recent Observational and Reanalysis Products. *Front. Clim.* **2022**, *4*, 989505. [CrossRef]
82. Soci, C.; Hersbach, H.; Simmons, A.; Poli, P.; Bell, B.; Berrisford, P.; Horányi, A.; Muñoz Sabater, J.; Nicolas, J.; Radu, R. The ERA5 Global Reanalysis From 1940 to 2022. *Q. J. R. Meteorol. Soc.* **2024**, *150*, 4014–4048. [CrossRef]
83. Wang, Q.; Xia, J.; She, D.; Zhang, X.; Liu, J.; Zhang, Y. Assessment of Four Latest Long-Term Satellite-Based Precipitation Products in Capturing the Extreme Precipitation and Streamflow Across a Humid Region of Southern China. *Atmos. Res.* **2021**, *257*, 105554. [CrossRef]
84. Ding, Y.; Wang, F.; Lu, Z.; Sun, P.; Wei, R.; Zhou, L.; Ao, T. Assessments of Various Precipitation Product Performances and Disaster Monitoring Utilities Over the Tibetan Plateau. *Sci. Rep.* **2024**, *14*, 19740. [CrossRef]
85. Satgé, F.; Pillot, B.; Roig, H.; Bonnet, M. Are Gridded Precipitation Datasets a Good Option for Streamflow Simulation Across the Juruá River Basin, Amazon? *J. Hydrol.* **2021**, *602*, 126773. [CrossRef]
86. Farr, T.G.; Rosen, P.A.; Caro, E.; Crippen, R.; Duren, R.; Hensley, S.; Kobrick, M.; Paller, M.; Rodriguez, E.; Roth, L. The Shuttle Radar Topography Mission. *Rev. Geophys.* **2007**, *45*, RG2004. [CrossRef]
87. Wang, X.; Zhou, J.; Ma, J.; Luo, P.; Fu, X.; Feng, X.; Zhang, X.; Jia, Z.; Wang, X.; Huang, X. Evaluation and Comparison of Reanalysis Data for Runoff Simulation in the Data-Scarce Watersheds of Alpine Regions. *Remote Sens.* **2024**, *16*, 751. [CrossRef]
88. Aryal, A.; Tran, T.; Kumar, B.; Lakshmi, V. Evaluation of Satellite-Derived Precipitation Products for Streamflow Simulation of a Mountainous Himalayan Watershed: A Study of Myagdi Khola in Kali Gandaki Basin, Nepal. *Remote Sens.* **2023**, *15*, 4762. [CrossRef]
89. Yuan, X.; Yang, K.; Lu, H.; He, J.; Sun, J.; Wang, Y. Characterizing the Features of Precipitation for the Tibetan Plateau Among Four Gridded Datasets: Detection Accuracy and Spatio-Temporal Variabilities. *Atmos. Res.* **2021**, *264*, 105875. [CrossRef]
90. Chen, Y.; Ding, M.; Zhang, G.; Wang, Y.; Li, J. Evaluation of ERA5 Reanalysis Precipitation Data in the Yarlung Zangbo River Basin of the Tibetan Plateau. *J. Hydrometeorol.* **2023**, *24*, 1491–1507. [CrossRef]
91. Wu, X.; Su, J.; Ren, W.; Lü, H.; Yuan, F. Statistical Comparison and Hydrological Utility Evaluation of ERA5-Land and IMERG Precipitation Products On the Tibetan Plateau. *J. Hydrol.* **2023**, *620*, 129384. [CrossRef]
92. Hu, X.; Yuan, W. Evaluation of ERA5 Precipitation Over the Eastern Periphery of the Tibetan Plateau From the Perspective of Regional Rainfall Events. *Int. J. Climatol.* **2021**, *41*, 2625–2637. [CrossRef]
93. Wang, R.; Liu, Y.; Wang, R.; Liu, Y.; Wu, X. Intercomparison of Reanalysis and Satellite Precipitation Products in Endorheic and Exorheic Basins On the Tibetan Plateau. *J. Hydrol. Reg. Stud.* **2024**, *56*, 102004. [CrossRef]
94. Spezza, A.; Diolaiuti, G.A.; Fugazza, D.; Maugeri, M.; Manara, V. Intercomparison of Gauge-Based, Reanalysis and Satellite Gridded Precipitation Datasets in High Mountain Asia: Insights From Observations and Discharge Data. *Climate* **2025**, *13*, 253. [CrossRef]
95. Li, H.; Cao, Y.; Guo, Y.; Zhou, C.; Wu, L.; Fan, C.; Yan, C.; Zhou, L. Comprehensive Evaluation of Multi-Version Global Satellite Mapping of Precipitation (GSMaP) Products Over the Qinghai–Tibetan Plateau. *Remote Sens.* **2026**, *18*, 1122. [CrossRef]
96. Yang, Y.; Ji, W.; Niu, L.; Zheng, Z.; Huang, W.; Zhang, C.; Hao, X.; Xiao, J.; Li, H. Assessing Satellite and Reanalysis-Based Precipitation Products in Cold and Arid Mountainous Regions. *J. Hydrol. Reg. Stud.* **2024**, *51*, 101612. [CrossRef]
97. Zhang, Y.; Huang, Y.; Xu, H.; Wang, S.; Long, T.; Zhao, Q. Evaluation of Precipitation Frequency and Intensity as Estimated by the GPM IMERG Precipitation Product at Daily and Hourly Scales Over the Tibetan Plateau. *Atmosphere* **2023**, *14*, 1653. [CrossRef]
98. Jia, J.; He, Y.; Zhang, B.; Huo, Z.; Tang, Z.; Wang, S.; Yu, H.; Guan, X. Evaluation of Hourly Summer Precipitation Products Over the Tibetan Plateau: A Comparative Analysis of IMERG, CMORPH, and TPHiPr. *Atmos. Res.* **2025**, *316*, 107955. [CrossRef]
99. Feng, Y.; Qi, Y.; Chen, D.; Li, D.; Li, Z.; Xu, X. Multi-Scale Analysis of Satellite, Reanalysis and Muti-Source Precipitation Estimates Over the Tibetan Plateau. *Atmos. Res.* **2024**, *309*, 107484. [CrossRef]
100. Shi, J.; Wang, B.; Wang, G.; Yuan, F.; Shi, C.; Zhou, X.; Zhang, L.; Zhao, C. Are the Latest GSMaP Satellite Precipitation Products Feasible for Daily and Hourly Discharge Simulations in the Yellow River Source Region? *Remote Sens.* **2021**, *13*, 4199. [CrossRef]
101. Zhang, Y.; Ju, Q.; Zhang, L.; Xu, C.; Lai, X. Evaluation and Hydrological Application of Four Gridded Precipitation Datasets Over a Large Southeastern Tibetan Plateau Basin. *Remote Sens.* **2022**, *14*, 2936. [CrossRef]
102. Wang, Y.; Sun, W.; Huai, B.; Wang, Y.; Ji, K.; Yang, X.; Du, W.; Qin, X.; Wang, L. Comparison and Evaluation of the Performance of Reanalysis Datasets for Compound Extreme Temperature and Precipitation Events in the Qilian Mountains. *Atmos. Res.* **2024**, *304*, 107375. [CrossRef]
103. Trenberth, K.E.; Zhang, Y.; Gehne, M. Intermittency in Precipitation: Duration, Frequency, Intensity, and Amounts Using Hourly Data. *J. Hydrometeorol.* **2017**, *18*, 1393–1412. [CrossRef]

104. Ma, H.Y.; Xie, S.; Boyle, J.S.; Klein, S.A.; Zhang, Y. Metrics and Diagnostics for Precipitation-Related Processes in Climate Model Short-Range Hindcasts. *J. Clim.* **2013**, *26*, 1516–1534. [CrossRef]
105. Feng, Y.; Qi, Y.; Zhao, Z.; Li, D. Can Satellite Or Reanalysis Precipitation Products Depict the Location and Intensity of Rainfall at Flash Flood Scale Over the Eastern Mountainous Area of the Tibetan Plateau? *Water Resour. Res.* **2024**, *60*, e2024WR037381. [CrossRef]
106. Cammalleri, C.; Sarwar, A.N.; Avino, A.; Nikravesh, G.; Bonaccorso, B.; Mendicino, G.; Senatore, A.; Manfreda, S. Testing Trends in Gridded Rainfall Datasets at Relevant Hydrological Scales: A Comparative Study with Regional Ground Observations in Southern Italy. *J. Hydrol. Reg. Stud.* **2024**, *55*, 101950. [CrossRef]
107. Shen, G.; Zeng, L.; Fu, L.; Wang, L.; Xiong, J.; Wang, W. An Effective Gauge-Satellite Fusion Approach for Daily Precipitation Bias Correction Based On Multi-Dimensional Precipitation Feature Space (BCFS). *Atmos. Res.* **2026**, *331*, 108624. [CrossRef]
108. Butcher, J.B.; Zi, T.; Pickard, B.R.; Job, S.C.; Johnson, T.E.; Groza, B.A. Efficient Statistical Approach to Develop Intensity-Duration-Frequency Curves for Precipitation and Runoff Under Future Climate. *Clim. Change* **2021**, *164*, 3. [CrossRef]
109. Liu, J.; Zhou, Y.; Lu, F.; Yu, Y.; Yan, D.; Hu, Y.; Xue, W. Evaluating Satellite- and Reanalysis-Based Precipitation Products Over the Qinghai-Tibetan Plateau in the Perspective of a New Error-Index System. *Int. J. Climatol.* **2023**, *43*, 2200–2219. [CrossRef]
110. Boushaki, F.I.; Hsu, K.; Sorooshian, S.; Park, G.; Mahani, S.; Shi, W. Bias Adjustment of Satellite Precipitation Estimation Using Ground-Based Measurement: A Case Study Evaluation Over the Southwestern United States. *J. Hydrometeorol.* **2009**, *10*, 1231–1242. [CrossRef]
111. Moazami, S.; Na, W.; Najafi, M.R.; de Souza, C. Spatiotemporal Bias Adjustment of IMERG Satellite Precipitation Data Across Canada. *Adv. Water Resour.* **2022**, *168*, 104300. [CrossRef]
112. Yang, Z.; Hsu, K.; Sorooshian, S.; Xu, X.; Braithwaite, D.; Verbist, K.M.J. Bias Adjustment of Satellite-Based Precipitation Estimation Using Gauge Observations: A Case Study in Chile. *J. Geophys. Res. Atmos.* **2016**, *121*, 3790–3806. [CrossRef]
113. Bodjrènou, R.; Sintondji, L.O.; Ahamidé, B.; N'Tcha M'Po, Y.; Gbaguidi, B.; Comandan, F. Challenges in Reliable Bias Correction of Hydro-Climatic and Energy Data: Towards a Reconstruction of Datasets. *Int. J. Appl. Earth Obs. Geoinf.* **2026**, *150*, 105362. [CrossRef]
114. Dinku, M.B.; Gibre, A.M. Comparison of Bias Correction Methods to Regional Climate Model Simulations for Climate Change Projection in Muger Subbasin, Upper Blue Nile Basin, Ethiopia. *J. Water Clim. Change* **2024**, *15*, 2612–2627. [CrossRef]
115. Tang, G.; Behrangi, A.; Long, D.; Li, C.; Hong, Y. Accounting for Spatiotemporal Errors of Gauges: A Critical Step to Evaluate Gridded Precipitation Products. *J. Hydrol.* **2018**, *559*, 294–306. [CrossRef]
116. Teutschbein, C.; Seibert, J. Bias Correction of Regional Climate Model Simulations for Hydrological Climate-Change Impact Studies: Review and Evaluation of Different Methods. *J. Hydrol.* **2012**, *456–457*, 12–29. [CrossRef]
117. Ma, J.; Wang, G.; Li, H. A Variance-Upscaling Quantile Mapping Method for Gridded Precipitation Bias Correction. *J. Hydrol.* **2024**, *632*, 130959. [CrossRef]
118. Byun, K.; Hamlet, A.F. An Improved Empirical Quantile Mapping Approach for Bias Correction of Extreme Values in Climate Model Simulations. *Environ. Res. Lett.* **2024**, *20*, 14041. [CrossRef]
119. Liu, S.; Raghavan, S.V.; Nguyen, N.S.; Ona, B.J.; Ngai, S.T.; Zhang, X. Improving the Regional Precipitation Simulation Corrected by Satellite Observation Using Quantile Mapping. *Remote Sens.* **2025**, *17*, 1716. [CrossRef]
120. Velasquez, P.; Messmer, M.; Raible, C.C. A New Bias-Correction Method for Precipitation Over Complex Terrain Suitable for Different Climate States: A Case Study Using WRF (Version 3.8.1). *Geosci. Model Dev.* **2020**, *13*, 5007–5027. [CrossRef]
121. Besharatifar, M.; Kamrani, S.; Nasseri, M. Augmenting Precipitation Datasets: A Comparative Study of Topographic-Based Corrections and Collocation Techniques Considering Orographic Effects. *Atmos. Res.* **2025**, *326*, 108317. [CrossRef]
122. Zhang, B.; Wang, S.; Moradkhani, H.; Slater, L.; Liu, J. A Vine Copula-Based Ensemble Projection of Precipitation Intensity–Duration–Frequency Curves at Sub-Daily to Multi-Day Time Scales. *Water Resour. Res.* **2022**, *58*, e2022WR032658. [CrossRef]
123. Pavlides, A.; Agou, V.D.; Hristopulos, D.T. Non-Parametric Kernel-Based Estimation and Simulation of Precipitation Amount. *J. Hydrol.* **2022**, *612*, 127988. [CrossRef]
124. Prodhan, F.A.; Zhang, J.; Hasan, S.S.; Pangali Sharma, T.P.; Mohana, H.P. A Review of Machine Learning Methods for Drought Hazard Monitoring and Forecasting: Current Research Trends, Challenges, and Future Research Directions. *Environ. Model. Softw.* **2022**, *149*, 105327. [CrossRef]
125. Dao, V.; Arellano, C.J.; Nguyen, P.; Almutlaq, F.; Hsu, K.; Sorooshian, S. Bias Correction of Satellite Precipitation Estimation Using Deep Neural Networks and Topographic Information Over the Western U.S. *J. Geophys. Res. Atmos.* **2025**, *130*, e2024JD042181. [CrossRef]
126. Ma, G.; Zhu, L.; Zhang, Y.; Huang, J.; Sun, Y.; Tian, W. Improvement of a Near-Real-Time Precipitation Estimation Algorithm Using Deep Learning. *IEEE Geosci. Remote Sens. Lett.* **2022**, *19*, 1006105. [CrossRef]
127. Wang, H.; Li, Z.; Zhang, T.; Chen, Q.; Guo, X.; Zeng, Q.; Xiang, J. Downscaling of GPM Satellite Precipitation Products Based On Machine Learning Method in Complex Terrain and Limited Observation Area. *Adv. Space Res.* **2023**, *72*, 2226–2244. [CrossRef]

128. Gan, F.; Diao, X.; Tan, K.; Li, X.; Cao, G.; Zhong, X.; Gao, Y. Error Correction for IMERG Precipitation Estimates Based On Climatological Adjustment Combining the Dry–Wet Season Division and Weight Allocation. *J. Hydrol.* **2023**, *624*, 129890. [CrossRef]
129. Baig, F.; Ali, L.; Faiz, M.A.; Chen, H.; Sherif, M. From Bias to Accuracy: Transforming Satellite Precipitation Data in Arid Regions with Machine Learning and Topographical Insights. *J. Hydrol.* **2025**, *653*, 132801. [CrossRef]
130. Bisht, D.S.; Preveen Kumar, D.; Amarjyothi, K.; Saha, U. Bias Correction of Satellite Precipitation Estimates Using Mumbai-MESONET Observations: A Random Forest Approach. *Atmos. Res.* **2025**, *315*, 107858. [CrossRef]
131. Belgiu, M.; Drăguţ, L. Random Forest in Remote Sensing: A Review of Applications and Future Directions. *ISPRS-J. Photogramm. Remote Sens.* **2016**, *114*, 24–31. [CrossRef]
132. Zhu, H.; Liu, H.; Zhou, Q.; Cui, A. A XGBoost-Based Downscaling-Calibration Scheme for Extreme Precipitation Events. *IEEE Trans. Geosci. Remote Sens.* **2023**, *61*, 4103512. [CrossRef]
133. Yu, Y.; Si, X.; Hu, C.; Zhang, J. A Review of Recurrent Neural Networks: LSTM Cells and Network Architectures. *Neural Comput.* **2019**, *31*, 1235–1270. [CrossRef]
134. Wang, H.; He, P.; Wang, G.; Bai, Y.; Li, Y. Downscaling and Bias Correction of ERA5-Land Precipitation over the Tibetan Plateau Using Terrain-Aware XGBoost. In Proceedings of the 2026 China Aerospace Information Technology Conference (CAIT), Wuzhen, China, 9–11 May 2026.
135. Le, X.; Lee, G.; Jung, K.; An, H.; Lee, S.; Jung, Y. Application of Convolutional Neural Network for Spatiotemporal Bias Correction of Daily Satellite-Based Precipitation. *Remote Sens.* **2020**, *12*, 2731. [CrossRef]
136. Beck, H.E.; Van Dijk, A.I.; Levizzani, V.; Schellekens, J.; Miralles, D.G.; Martens, B.; De Roo, A. MSWEP: 3-Hourly 0.25° Global Gridded Precipitation (1979–2015) by Merging Gauge, Satellite, and Reanalysis Data. *Hydrol. Earth Syst. Sci.* **2017**, *21*, 589–615. [CrossRef]
137. Ma, Y.; Hong, Y.; Chen, Y.; Yang, Y.; Tang, G.; Yao, Y.; Long, D.; Li, C.; Han, Z.; Liu, R. Performance of Optimally Merged Multisatellite Precipitation Products Using the Dynamic Bayesian Model Averaging Scheme Over the Tibetan Plateau. *J. Geophys. Res. Atmos.* **2018**, *123*, 814–834. [CrossRef]
138. Ma, Y.; Yang, Y.; Han, Z.; Tang, G.; Maguire, L.; Chu, Z.; Hong, Y. Comprehensive Evaluation of Ensemble Multi-Satellite Precipitation Dataset Using the Dynamic Bayesian Model Averaging Scheme Over the Tibetan Plateau. *J. Hydrol.* **2018**, *556*, 634–644. [CrossRef]
139. Ma, Y.; Sun, X.; Chen, H.; Hong, Y.; Zhang, Y. A Two-Stage Blending Approach for Merging Multiple Satellite Precipitation Estimates and Rain Gauge Observations: An Experiment in the Northeastern Tibetan Plateau. *Hydrol. Earth Syst. Sci.* **2021**, *25*, 359–374. [CrossRef]
140. Dou, Y.; Shi, K.; Cai, H.; Xie, M.; Liu, R. Review of Utilisation Methods of Multi-Source Precipitation Products for Flood Forecasting in Areas with Insufficient Rainfall Gauges. *Atmosphere* **2025**, *16*, 835. [CrossRef]
141. Zhao, Y.; Xu, K.; Dong, N.; Wang, H. Optimally Integrating Multi-Source Products for Improving Long Series Precipitation Precision by Using Machine Learning Methods. *J. Hydrol.* **2022**, *609*, 127707. [CrossRef]
142. He, J.; Yang, K.; Tang, W.; Lu, H.; Qin, J.; Chen, Y.; Li, X. The First High-Resolution Meteorological Forcing Dataset for Land Process Studies Over China. *Sci. Data* **2020**, *7*, 25. [CrossRef]
143. Zhao, K.; Zhong, S. Evaluation and Error Analysis of Multi-Source Precipitation Datasets During Summer Over the Tibetan Plateau. *Atmosphere* **2024**, *15*, 165. [CrossRef]
144. Tian, F.; Hou, S.; Yang, L.; Hu, H.; Hou, A. How Does the Evaluation of the GPM IMERG Rainfall Product Depend On Gauge Density and Rainfall Intensity? *J. Hydrometeorol.* **2018**, *19*, 339–349. [CrossRef]
145. Lyu, F.; Tang, G.; Behrangi, A.; Wang, T.; Tan, X.; Ma, Z.; Xiong, W. Precipitation Merging Based On the Triple Collocation Method Across Mainland China. *IEEE Trans. Geosci. Remote Sens.* **2021**, *59*, 3161–3176. [CrossRef]
146. Li, C.; Tang, G.; Hong, Y. Cross-Evaluation of Ground-Based, Multi-Satellite and Reanalysis Precipitation Products: Applicability of the Triple Collocation Method Across Mainland China. *J. Hydrol.* **2018**, *562*, 71–83. [CrossRef]
147. Stoffelen, A. Toward the True Near-Surface Wind Speed: Error Modeling and Calibration Using Triple Collocation. *J. Geophys. Res. Oceans* **1998**, *103*, 7755–7766. [CrossRef]
148. Wu, X.; Zhu, J.; Lai, C. Assessment and Data Fusion of Satellite-Based Precipitation Estimation Products Over Ungauged Areas Based On Triple Collocation without in Situ Observations. *Remote Sens.* **2023**, *15*, 4210. [CrossRef]
149. Dong, J.; Wei, L.; Chen, X.; Duan, Z.; Lu, Y. An Instrument Variable Based Algorithm for Estimating Cross-Correlated Hydrological Remote Sensing Errors. *J. Hydrol.* **2020**, *581*, 124413. [CrossRef]
150. Su, C.H.; Ryu, D.; Crow, W.T.; Western, A.W. Beyond Triple Collocation: Applications to Soil Moisture Monitoring. *J. Geophys. Res. Atmos.* **2014**, *119*, 6419–6439. [CrossRef]
151. Yilmaz, M.T.; Crow, W.T. Evaluation of Assumptions in Soil Moisture Triple Collocation Analysis. *J. Hydrometeorol.* **2014**, *15*, 1293–1302. [CrossRef]

152. Wei, L.; Jiang, S.; Ren, L.; Yuan, S.; Liu, Y.; Yang, X.; Wang, M.; Zhang, L.; Yu, H.; Duan, Z. An Extended Triple Collocation Method with Maximized Correlation for Near Global-Land Precipitation Fusion. *Geophys. Res. Lett.* **2023**, *50*, e2023GL105120. [CrossRef]
153. Wei, L.; Jiang, S.; Dong, J.; Ren, L.; Yong, B.; Yang, B.; Li, X.; Duan, Z. A Combined Extended Triple Collocation and Cumulative Distribution Function Merging Framework for Improved Daily Precipitation Estimates Over Mainland China. *J. Hydrol.* **2024**, *641*, 131757. [CrossRef]
154. Jing, W.; Yang, Y.; Yue, X.; Zhao, X. A Spatial Downscaling Algorithm for Satellite-Based Precipitation Over the Tibetan Plateau Based On NDVI, DEM, and Land Surface Temperature. *Remote Sens.* **2016**, *8*, 655. [CrossRef]
155. Jia, S.; Zhu, W.; Lű, A.; Yan, T. A Statistical Spatial Downscaling Algorithm of TRMM Precipitation Based On NDVI and DEM in the Qaidam Basin of China. *Remote Sens. Environ.* **2011**, *115*, 3069–3079. [CrossRef]
156. Hong, Z.; Han, Z.; Li, X.; Long, D.; Tang, G.; Wang, J. Generation of an Improved Precipitation Data Set From Multisource Information Over the Tibetan Plateau. *J. Hydrometeorol.* **2021**, *1*, 1275–1295. [CrossRef]
157. Shi, X.; Chen, Z.; Wang, H.; Yeung, D.; Wong, W.; Woo, W. Convolutional LSTM Network: A Machine Learning Approach for Precipitation Nowcasting. In Proceedings of the Advances in Neural Information Processing Systems 28 (NIPS 2015), Montréal, QC, Canada, 7–12 December 2015.
158. Fang, W.; Qin, H.; Liu, G.; Yang, X.; Xu, Z.; Jia, B.; Zhang, Q. A Method for Spatiotemporally Merging Multi-Source Precipitation Based On Deep Learning. *Remote Sens.* **2023**, *15*, 4160. [CrossRef]
159. Vaswani, A.; Shazeer, N.; Parmar, N.; Uszkoreit, J.; Jones, L.; Gomez, A.N.; Kaiser, A.; Polosukhin, I. Attention is All You Need. In Proceedings of the Advances in Neural Information Processing Systems 30 (NIPS 2017), Long Beach, CA, USA, 4–9 December 2017.
160. Bodnar, C.; Bruinsma, W.P.; Lucic, A.; Stanley, M.; Allen, A.; Brandstetter, J.; Garvan, P.; Riechert, M.; Weyn, J.A.; Dong, H.; et al. A Foundation Model for the Earth System. *Nature* **2025**, *641*, 1180–1187. [CrossRef]
161. Pan, S.J.; Yang, Q. A Survey On Transfer Learning. *IEEE Trans. Knowl. Data Eng.* **2009**, *22*, 1345–1359. [CrossRef]
162. Liu, Z.; Yang, Q.; Shao, J.; Wang, G.; Liu, H.; Tang, X.; Xue, Y.; Bai, L. Improving Daily Precipitation Estimation in the Data Scarce Area by Merging Rain Gauge and TRMM Data with a Transfer Learning Framework. *J. Hydrol.* **2022**, *613*, 128455. [CrossRef]
163. Shwartz-Ziv, R.; Armon, A. Tabular Data: Deep Learning is Not All You Need. *Inf. Fusion.* **2022**, *81*, 84–90. [CrossRef]
164. Hu, B.; Zhang, X.; Fang, Y.; Mou, S.; Qian, R.; Li, J.; Chen, Z. Multisource Precipitation Data Merging Using a Dual-Layer ConvLSTM Model. *Remote Sens.* **2025**, *17*, 546. [CrossRef]
165. Lei, H.; Zhao, H.; Ao, T. Ground Validation and Error Decomposition for Six State-of-the-Art Satellite Precipitation Products Over Mainland China. *Atmos. Res.* **2022**, *269*, 106017. [CrossRef]
166. Milani, L.; Kidd, C. The State of Precipitation Measurements at Mid-to-High Latitudes. *Atmosphere* **2023**, *14*, 1677. [CrossRef]
167. He, K.; Ma, Z.; Li, S.; Chen, T.; Xu, T.; Li, L.; Jiang, X.; Wang, T. A Thermodynamically Informed Precipitation Retrieval Method Based On FY-4a/AGRI Multi-Channel Infrared Observations Over Complex Terrain. *Geophys. Res. Lett.* **2025**, *52*, e2025GL117433. [CrossRef]
168. Chen, S.; Li, L.; Wei, Z.; Wei, N.; Zhang, Y.; Zhang, S.; Yuan, H.; Shangguan, W.; Zhang, S.; Li, Q. Exploring Topography Downscaling Methods for Hyper-Resolution Land Surface Modeling. *J. Geophys. Res. Atmos.* **2024**, *129*, e2024JD041338. [CrossRef]
169. Li, H.; Chen, J.; Li, L. A Two-Step Machine Learning Framework for Incorporating Spatial Information Into Multi-Source Precipitation Merging Over High-Alpine Regions. *Sci. China Earth Sci.* **2026**, *69*, 2074–2089. [CrossRef]
170. Song, P.; Liu, G. Partitioning Solid and Liquid Precipitation Over the Tibetan Plateau Based On Satellite Radar Observations. *J. Hydrometeorol.* **2021**, *1*, 2861–2875. [CrossRef]
171. Miao, C.; Immerzeel, W.W.; Xu, B.; Yang, K.; Duan, Q.; Li, X. Understanding the Asian Water Tower Requires a Redesigned Precipitation Observation Strategy. *Proc. Natl. Acad. Sci. USA* **2024**, *121*, e1891410175. [CrossRef]
172. Skofronick-Jackson, G.; Petersen, W.A.; Berg, W.; Kidd, C.; Stocker, E.F.; Kirschbaum, D.B.; Kakar, R.; Braun, S.A.; Huffman, G.J.; Iguchi, T. The Global Precipitation Measurement (GPM) Mission for Science and Society. *Bull. Am. Meteorol. Soc.* **2017**, *98*, 1679–1695. [CrossRef]
173. Pradhan, R.K.; Markonis, Y.; Vargas Godoy, M.R.; Villalba-Pradas, A.; Andreadis, K.M.; Nikolopoulos, E.I.; Papalexiou, S.M.; Rahim, A.; Tapiador, F.J.; Hanel, M. Review of GPM IMERG Performance: A Global Perspective. *Remote Sens. Environ.* **2022**, *268*, 112754. [CrossRef]
174. Davis, C.; Brown, B.; Bullock, R. Object-Based Verification of Precipitation Forecasts. Part I: Methodology and Application to Mesoscale Rain Areas. *Mon. Weather Rev.* **2006**, *134*, 1772–1784. [CrossRef]
175. Antonio, B.; Aitchison, L. How to Derive Skill From the Fractions Skill Score. *Mon. Weather Rev.* **2025**, *153*, 1021–1033. [CrossRef]
176. Roberts, N.M.; Lean, H.W. Scale-Selective Verification of Rainfall Accumulations From High-Resolution Forecasts of Convective Events. *Mon. Weather Rev.* **2008**, *136*, 78–97. [CrossRef]
177. Davis, C.A.; Brown, B.G.; Bullock, R.; Halley-Gotway, J. The Method for Object-Based Diagnostic Evaluation (MODE) Applied to Numerical Forecasts From the 2005 NSSL/SPC Spring Program. *Weather Forecast.* **2009**, *24*, 1252–1267. [CrossRef]

178. Kazamias, A.; Sapountzis, M.; Lagouvardos, K. Evaluation of GPM-IMERG Rainfall Estimates at Multiple Temporal and Spatial Scales Over Greece. *Atmos. Res.* **2022**, *269*, 106014. [CrossRef]
179. Chen, F.; Gao, Y.; Wang, Y.; Li, X. A Downscaling-Merging Method for High-Resolution Daily Precipitation Estimation. *J. Hydrol.* **2020**, *581*, 124414. [CrossRef]
180. Wolvin, S.; Strong, C.; Rupper, S.; Steenburgh, W.J. Climatology of Orographic Precipitation Gradients Over High Mountain Asia Derived From Dynamical Downscaling. *J. Geophys. Res. Atmos.* **2024**, *129*, e2024JD041010. [CrossRef]
181. Lundquist, J.; Abel, M.R.; Gutmann, E.; Kapnick, S. Our Skill in Modeling Mountain Rain and Snow is Bypassing the Skill of Our Observational Networks. *Bull. Am. Meteorol. Soc.* **2019**, *100*, 2473–2490. [CrossRef]
182. Chang, Y.; Qi, Y.; Wang, Z. Comprehensive Evaluation of IMERG, ERA5-Land and their Fusion Products in the Hydrological Simulation of Three Karst Catchments in Southwest China. *J. Hydrol. Reg. Stud.* **2024**, *52*, 101671. [CrossRef]
183. Wang, P.; Bai, X.; Wu, X.; Lai, C.; Zhang, Z. Spatially Continuous Assessment of Satellite-Based Precipitation Products Using Triple Collocation Approach and Discrete Gauge Observations Via Geographically Weighted Regression. *J. Hydrol.* **2022**, *608*, 127640. [CrossRef]
184. Alemohammad, S.H.; McColl, K.A.; Konings, A.G.; Entekhabi, D.; Stoffelen, A. Characterization of Precipitation Product Errors Across the United States Using Multiplicative Triple Collocation. *Hydrol. Earth Syst. Sci.* **2015**, *19*, 3489–3503. [CrossRef]
185. Zhao, S.; Xiong, Z.; Zhu, X.X. RainScaler: A Physics-Inspired Network for Precipitation Correction and Downscaling. *IEEE Trans. Geosci. Remote Sens.* **2025**, *63*, 4105318. [CrossRef]
186. Meema, T.; Wattanasetpong, J.; Wichakul, S. Integrating Machine Learning and Zoning-Based Techniques for Bias Correction in Gridded Precipitation Data to Improve Hydrological Estimation in the Data-Scarce Region. *J. Hydrol.* **2025**, *646*, 132356. [CrossRef]
187. Wu, H.; Yang, Q.; Liu, J.; Wang, G. A Spatiotemporal Deep Fusion Model for Merging Satellite and Gauge Precipitation in China. *J. Hydrol.* **2020**, *584*, 124664. [CrossRef]
188. Deng, L.; Zhang, X.; Slater, L.J.; Liu, H.; Tao, S. Integrating Euclidean and Non-Euclidean Spatial Information for Deep Learning-Based Spatiotemporal Hydrological Simulation. *J. Hydrol.* **2024**, *638*, 131438. [CrossRef]
189. Chen, C.; He, Q.; Li, Y. Downscaling and Merging Multiple Satellite Precipitation Products and Gauge Observations Using Random Forest with the Incorporation of Spatial Autocorrelation. *J. Hydrol.* **2024**, *632*, 130919. [CrossRef]
190. Avino, A.; Cimorelli, L.; Furcolo, P.; Noto, L.V.; Pelosi, A.; Pianese, D.; Villani, P.; Manfreda, S. Are Rainfall Extremes Increasing in Southern Italy? *J. Hydrol.* **2024**, *631*, 130684. [CrossRef]
191. Williams, C.J.R.; Kniveton, D.R. Atmosphere-Land Surface Interactions and their Influence On Extreme Rainfall and Potential Abrupt Climate Change Over Southern Africa. *Clim. Change* **2012**, *112*, 981–996. [CrossRef]
192. Yao, N.; Ye, J.; Wang, S.; Yang, S.; Lu, Y.; Zhang, H.; Yang, X. Bias Correction of the Hourly Satellite Precipitation Product Using Machine Learning Methods Enhanced with High-Resolution WRF Meteorological Simulations. *Atmos. Res.* **2024**, *310*, 107637. [CrossRef]
193. Yang, Y.; Han, W.; Sun, H.; Li, J.; Yan, J.; Gao, Z. Reconstruction of 3D Precipitation Measurements From FY-3G MWRI-RM Imaging and Sounding Channels. *Atmos. Meas. Tech.* **2025**, *18*, 4249–4269. [CrossRef]
194. Moldovan, G.; Pinnington, E.; Prieto Nemesio, A.; Lang, S.; Ben Bouallègue, Z.; Dramsch, J.; Alexe, M.; Santa Cruz, M.; Hahner, S.; Cook, H. AIFS Single 1.1. 0: An Update to ECMWF's Machine-Learned Weather Forecast Model AIFS. *Geosci. Model Dev.* **2026**, *19*, 4703–4724.
195. Lam, R.; Sanchez-Gonzalez, A.; Willson, M.; Wirnsberger, P.; Fortunato, M.; Alet, F.; Ravuri, S.; Ewalds, T.; Eaton-Rosen, Z.; Hu, W. Learning Skillful Medium-Range Global Weather Forecasting. *Science* **2023**, *382*, 1416–1421. [CrossRef]
196. Wu, X.; Lu, G.; Wu, Z. Remote Sensing Technology in the Construction of Digital Twin Basins: Applications and Prospects. *Water* **2023**, *15*, 2040. [CrossRef]